Stream Network Dynamics in Three Watersheds in the Southeastern USA Highlight Interactions Between Physiographic Variables

Delaney M. Peterson [1,2], C. Nathan Jones [1], Kaci Zarek [1,3], Michelle Wolford [1], Chelsea R. Smith [1], Charles T. Bond [4], Stephen Plont [1,5], Maggi Kraft [6], Shannon Speir [7], Sam Zipper [8,9], Sarah E. Godsey [6], Jonathan P. Benstead [1], Arial J. Shogren [1], Kevin A. Kuehn [4], and Carla L. Atkinson [1]

[1] Department of Biological Sciences, University of Alabama, Tuscaloosa, AL, USA.

[2] Department of Biological and Ecological Engineering, Oregon State University, Corvallis, OR, USA.

[3] Department of Ecology and Evolutionary Biology, Cornell University, Ithaca, NY, USA.

[4] School of Biological, Environmental, and Earth Sciences, University of Southern Mississippi, Hattiesburg, MS, USA.

[5] Odum School of Ecology, University of Georgia, Athens, GA, USA.

[6] Department of Geosciences, Idaho State University, Pocatello, ID, USA.

[7] Department of Crop, Soil, and Environmental Sciences, University of Arkansas, Fayetteville, AR, USA.

[8] Kansas Geological Survey, University of Kansas, Lawrence, KS, USA.

[9] Department of Geology, University of Kansas, Lawrence, KS, USA.

Corresponding Author: Delaney Peterson (dmpeterson2@crimson.ua.edu)

<u>This is a non-peer-reviewed manuscript being submitted to Hydrological Processes</u>

Abstract

Non-perennial streams, which cease flowing regularly across time or space, comprise ~60% of the global river network and play an important role in the physical, chemical, and biological functions of downstream waters. However, predicting their network extent and its spatiotemporal variability remains a key challenge across regulatory, practitioner, and research communities, especially given that most investigations to date have focused on high-relief watersheds. To address this challenge, we investigated the spatial and temporal patterns of stream wetting and drying within the context of landscape characteristics. We instrumented three headwater stream networks located in the Coastal Plain, Piedmont, and

Appalachian Plateaus regions in the southeastern United States. In each network, we used ≥ 20 water presence/absence sensors over two water-years (2023 and 2024) to investigate seasonal and interannual variability in network extent. Across the physiographic provinces, we found that a combination of topographic, geologic, and vegetative drivers best explained variability in stream network persistence. Specifically, key drivers in the Coastal Plain were topographic convergence and channel incision, in the Piedmont were channel slope, depth to bedrock, and coniferous canopy cover, and in the Appalachian Plateaus were cave-spring presence and depth to bedrock. Our results also emphasized the role that sensor placement plays in understanding network-scale patterns, as deploying sensors in areas of greatest hydrologic variability was crucial to capturing the full range of network expansion, contraction, and fragmentation. This study demonstrated that low-relief stream networks have complex drivers of network extent dynamics, and that consideration of other factors such as soils and vegetation in addition to topography can help explain network expansion and contraction in low-relief headwater networks.

Keywords: stream extent, physiography, low-relief, non-perennial streams, watersheds.

1. INTRODUCTION

Streams are dynamic features on the landscape (Godsey & Kirchner, 2014) that respond to inputs from precipitation and subsurface storage zones, causing variation in streamflow and network extent at daily to decadal scales. Non-perennial streams are portions of the stream network that cease flowing regularly across either space or time (Busch et al., 2020), often in headwater segments of the network that expand and contract dynamically. Non-perennial streams constitute at least 60% of global river networks (Messager et al., 2021) and have important impacts on downstream reaches (Brinkerhoff et al., 2024; Zimmer et al., 2022) including providing diverse habitat (e.g., Datry et al., 2018), generating unique biogeochemical signals (e.g., Bernal et al., 2019; Gómez-Gener et al., 2021; Zarek et al., 2025), and contributing to seasonal flow and groundwater recharge (e.g., Zimmer & McGlynn, 2017). However, our understanding of the patterns of network expansion, contraction, and fragmentation and the processes they control has been biased towards quantifying patterns in streamflow variability at the watershed outlet, rather than across the network (but see Botter & Durighetto, 2020; Godsey & Kirchner, 2014; Prancevic et al., 2025). Therefore, identifying the primary drivers of variability in network extent across systems is required to predict how non-perennial streams drive spatiotemporal variation in network connectivity.

Watershed physiographic characteristics exert strong control over hydrologic processes and network extent. Many studies have documented how climate, geology, and land cover act as first-order controls on streamflow and network extent across river systems (Costigan et al., 2016; Hynes, 1975; Zipper et al., 2021). Additionally, recent investigations have highlighted the role of watershed topography, suggesting that landscape features like flow convergence and valley transmissivity drive patterns in network expansion and contraction by regulating both the volume of subsurface storage and rate of down-valley flow (Godsey & Kirchner, 2014; Prancevic & Kirchner, 2019). However, other studies have found that finer spatial-scale heterogeneity in physiographic characteristics such as local bedrock permeability and spring abundance (Crowther et al., 2026), soil properties (Gutiérrez-Jurado et al., 2019; Warix et al., 2023), or riparian vegetation (Newcomb & Godsey, 2023) can exert stronger controls on network extent dynamics than topography. Further, these heterogeneities are more difficult to measure than larger watershed-scale properties, limiting our ability to effectively predict network extent dynamics. Therefore, a clear picture of the drivers of flowing network extent, potential interactions among them, and how these drivers and interactions vary across watersheds is lacking.

Our current understanding of network expansion and contraction is also biased toward temporally low-resolution measurements from high-relief watersheds. A large proportion of hydrologic research has been conducted in temperate, high-relief locations (Burt & McDonnell, 2015), including those studying network expansion and contraction (e.g., van Meerveld et al., 2019; Ward et al., 2018). Moreover, many of these network dynamics studies use spatially high-resolution network mapping techniques (hereafter, stream-walking; Godsey & Kirchner, 2014). While stream-walking provides a spatially dense representation of the flowing channel, temporal resolution is typically limited to seasonal measurements. Recent advancements in low-cost sensors (see Jensen et al., 2019) help bridge this gap by providing temporally dense point measures of water presence or absence across a network. However, sensor placement strategies are optimized for individual study objectives, making it difficult to synthesize these point observations into expansion, contraction, and fragmentation dynamics across different studies and networks. Therefore, comparable sensor-based approaches in more diverse physiographic settings are needed to better characterize the landscape drivers of network dynamics.

To quantify the effects of landscape characteristics on network extent and variability, we focus on hydrologic connectivity, defined as the water-mediated movement of materials, organisms, and energy (Pringle, 2001; Rinderer et al., 2018). Hydrologic connectivity generally incorporates flows across vertical, lateral, and longitudinal dimensions, as well as through time (Harvey & Gooseff, 2015; Ward, 1989; Zimmer & McGlynn, 2018), providing a unifying framework for evaluating water fluxes across spatiotemporal scales as well as disciplines (Jones et al., 2019). Here, we focus on connectivity in the longitudinal dimension at the watershed scale, and define this connectivity as network expansion, contraction, and fragmentation through time. While many studies have paired longitudinal connectivity with observations of discharge at the outlet to investigate the impacts of flow and network variability on biogeochemical fluxes (e.g., Zarek et al., 2025; Zimmer & McGlynn, 2018), fewer studies have focused on the dynamics of longitudinal connectivity as an integrator of within-watershed hydrologic processes.

The goal of this study was to investigate the interactions between network extent dynamics and watershed characteristics in predominantly low-relief settings. In the southeastern USA, a natural gradient of topographic, geologic, and vegetative characteristics exists within a generally uniform climate, as much of the region receives similar precipitation inputs. Therefore, to test potential drivers of network connectivity, we instrumented three watersheds in the southeastern USA as representatives of a subset of these different landscapes – one each in the Coastal Plain, Piedmont, and Appalachian Plateaus regions. We deployed a standardized network of water presence/absence sensors in each watershed, and used these to monitor site- and network-scale flow dynamics across two water-years of contrasting dryness (2023 and 2024). We used this sensor network to address our research objectives: to (i) characterize the spatial and temporal patterns of network connectivity across a relatively low-relief region, (ii) investigate the role watershed topographic, geologic, and vegetative characteristics play in watershed-scale network expansion, contraction, and fragmentation, and (iii) evaluate the role of sensor placement in network-scale metrics of connectivity.

2. DATA AND METHODS

2.1 Site Descriptions

We instrumented three watersheds in Alabama (USA; Figure 2B) that were representative of their larger physiographic province, and that also contained non-perennial, headwater segments. Our watersheds were small and generally similar in size with comparable climatic settings and standardized sensor placement (Figure 2A; see *Section 2.2.1*), allowing us to investigate watershed controls across regions without confounding climatic or methodological factors. These watersheds all had a humid subtropical climate, with a mean annual precipitation ranging from 1,350 to 1,400 mm per year, and mean annual air temperatures ranging from 15.3 to 17.8˚C (Table 1; NOAA NCEI, 2025). This region receives generally consistent precipitation throughout the year with no obvious climatic dry season, though there is considerable intra- and interannual variability. For example, precipitation was below average across the region during the 2023-2024 study period, yet was above average the previous water-year (2022). High evapotranspiration (ET) rates in the late summer and early autumn drive reductions in streamflow and a hydrologic dry season in this region (Czikowsky & Fitzjarrald, 2004; Hupp, 2000). Additional information about these watersheds can be found in Text S1 and Plont et al. (2026).

Table 1. Watershed Characteristics

Research watershed	Outlet location (Lat., Lon.)	Mean Jan. air temp. [˚C][a]	Mean Jul. air temp. [˚C][a]	Mean annual precip. (mm/yr)[a]	Elevation range (masl), (relief, m)	Water-shed area (km^2)	Watershed average (min., max.) slope (%)	Primary lithology	Primary soil texture[b]
Appalachian Plateaus	34.968617, -86.165017	4.4˚	25.4˚	1,390	211 - 550 (339)	2.97	17 % (0.01, 69)	Karstic sedimentary	Silty clay loam
Piedmont	33.762197, -85.595507	5.3˚	25.3˚	1,400	345 - 456 (111)	0.92	12 % (0.005, 49)	Low-grade fractured metamorphic	Silt loam
Coastal Plain	32.984109, -88.013343	7.3˚	27.4˚	1,350	63 - 94 (31)	0.70	7 % (0.001, 28)	Sedimentary marine deposits	Fine, sometimes sandy, loam

[a]Obtained from NOAA NCEI (2025).

[b]Obtained from Soil Survey Staff (2025).

2.1.1 Appalachian Plateaus research watershed

The Appalachian Plateaus watershed drains a non-perennial tributary of Burks Creek in Jackson County, AL (Figure 2C). There were 1,350 mm and 1,300 mm of precipitation in the 2023 and 2024 water-year, respectively. This watershed has the highest relief of our three study sites, and is underlain by karstic Mississippian-aged sedimentary lithologic units (Table 1). In the headwaters, there are abundant cave-springs at the exposure of the Bangor limestone unit, as well as spring discharges from numerous fractures (Ponta, 2018). This watershed is characterized by generally steep stony slopes and shallow soils (Swenson, 1954). The upper portions of the watershed have thin, organic soils primarily in the Mollisol soil order, and the streambeds are primarily exposed bedrock. Conversely, the soils in the lower portions are highly weathered Ultisols, and stream sediment aggradation occurs (Soil Survey Staff, 2025). This watershed is primarily forested with deciduous species (Figure S1), and is privately owned and managed for hunting and conservation. This watershed, like much of the area, was used for silvicultural harvest until the turn of the 20th century, resulting in a mixed-age forest (Swenson, 1954). Additionally, portions of the valley bottom and several areas in the headwaters have been cleared for cultivation, but the majority of the riparian zone is forested.

2.1.2 Piedmont research watershed

The Piedmont watershed drains a non-perennial tributary to Pendergrass Creek in Cleburne County, AL (Figure 2D). There were 1,400 mm and 1,390 mm of precipitation in the 2023 and 2024 water-year, respectively. This network has moderate relief, and is underlain by Silurian-Devonian-aged low-grade metamorphic lithologic units that have formed highly weathered soils (Table 1). The groundwater systems in this region are complex due to the fractured lithology. The primary lithologic unit in this watershed is included in the metasedimentary and metavolcanic unconfined aquifer system (Kopaska-Merkel et al., 2000). This watershed is dominated by Ultisols. The upper portions of the watershed have thin and rocky soils where the regolith is close to the surface (Feminella, 1996; Kopaska-Merkel et al., 2000), with primarily coarse stream sediment (gravel, pebbles, and cobbles). Conversely, the lower portion of the watershed has deeper argillic soils, and the streambeds consist of a mix of coarse and fine-grained (sand, silt) sediment (Zarek et al., 2025). This watershed is entirely forested with mixed deciduous and coniferous species within the federally owned Talladega National Forest (Figure S2), and is managed for recreation, silviculture, and conservation.

2.1.3 Coastal Plain research watershed

The Coastal Plain watershed drains a non-perennial tributary to Shambley Creek in Greene County, AL (Figure 2E). There were 1,450 mm and 1,250 mm of precipitation in the 2023 and 2024 water-year, respectively. This watershed has the lowest relief in our study, and is underlain by Upper Cretaceous-age sedimentary lithologic units that are composed primarily of sand and clay (Table 1). The watershed is dominated by Ultisols, Alfisols with argillic horizons, and poorly organized Entisols (Soil Survey Staff, 2025). The stream substrate is primarily fine-grained sediment (clay lenses, silt, sand), with some conglomerate pebbles near the watershed outlet. Further, over half (55%) of the network is incised > 0.5 m below the riparian zone, and some areas of incision are nearly 2 m deep. This watershed is entirely forested with mixed coniferous and deciduous species (Figure S3), and managed for rotational silvicultural harvest by the Weyerhaeuser Company. Within this watershed, the uplands are almost entirely pine species, with dense riparian vegetation dominated by oaks. The southern upland portion of the watershed was harvested in the summer of 2024, but all vegetation within 11 m of the stream channel was preserved.

2.1.4 Within-watershed Hydrogeomorphic Features (HGFs)

We delineated each watershed into subunits linked to their hydrologic functions (hydrogeomorphic features, HGFs; following Peterson et al., 2025) to characterize the inherent variability of river corridor structure within our watersheds. Each HGF was assigned based on key structures within the river corridor that we identified in the field as potential regulators of hydrologic connectivity. In the Appalachian Plateaus, we delineated the network into two HGFs; HGF A1 was characterized by bedrock channels and steep slopes, and HGF A2 consisted of lower-gradient channels with sediment accumulation (Figure S4). In the Piedmont, we delineated the network into three units; HGF P1 had highly constrained valleys and steep slopes, HGF P2 consisted of wider valleys with coarse sediment, and HGF P3 was characterized by wide and densely vegetated riparian zones with low slopes (Figure S5). In the Coastal Plain, where the HGF framework was developed in Peterson et al. (2025), we delineated the network into three units; HGF C1 was defined as low-gradient reaches with high width-depth ratios, HGF C2 consisted of channels with distinct banks and evidence of over-bank flows, and HGF C3 had deeply entrenched (> 0.5 m of incision) channels that rarely inundated the adjacent riparian zone (Figure S6). By defining these HGFs as subunits of each watershed, we were able to aggregate individual sites into similar groups to evaluate watershed characteristics from data only available at larger scales (e.g., soils, geologic data).

2.2 Hydrologic Monitoring Instrumentation

We instrumented each watershed with a network of water presence/absence sensors to quantify network extent across time, as well as water persistence at each site. We also installed a discharge monitoring station at the watershed outlet, and collected local meteorological data using a weather station located within 5 km of the watershed outlet. All sensors logged at concurrent 15-minute intervals from 1 Oct. 2022 through the spring of 2024, and then logged at concurrent hourly intervals from the spring of 2024 through Sep. 2024.

2.2.1 Watershed-Scale Network Extent Monitoring

Each watershed was instrumented with 20 Stream Temperature, Intermittency, and Conductivity (hereafter, STIC) sensors that measured water presence/absence (Chapin et al., 2014; Jensen et al., 2019). We used a standardized site selection design based on the relationship between contributing area and topographic wetness index (TWI; Zipper et al., 2025) to maximize comparability across networks. This resulted in sensor networks that spanned a gradient of TWI, rather than a uniform density (Figure 1A-B). For an 11-month period (May 2022 through April 2023), we deployed an additional 29 STICs in the Piedmont to capture a higher spatial resolution and extent of conditions across the watershed in coordination with a large synoptic sampling effort (June 2022; see Plont et al., 2026). These additional STIC sensors were placed strategically to fill spatial gaps in the existing network while also expanding into the upstream ephemeral segments. At each site, we placed STIC sensors in the thalweg at the head of a riffle within the reach selected by the standardized site design (Figure 1C). Sensors were anchored within 1 cm of the stream bed to capture low flows. We maintained and downloaded data from the sensors every 4-6 months and removed the sensors for 3-7 days to change the batteries every 9 months. During every maintenance visit, we also recorded water presence/absence at the site and height of the sensor relative to the streambed to validate sensor measurements.

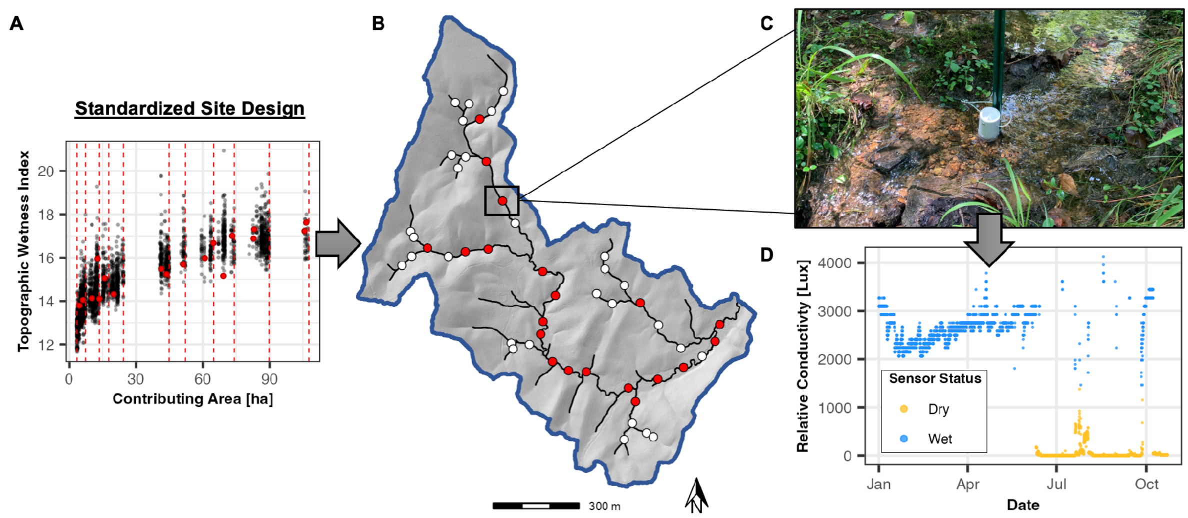

Figure 1. Standardized site design for sensor placement within each network. (A) The distribution of cells within the watershed raster, binned by contributing area. Selected points are indicated in red. (B) The Piedmont watershed, with the selected site locations indicated in red. The additional 29 strategic locations are indicated in white. (C) An image of a STIC deployed in a stream reach. (D) An example output from the STIC, with relative conductivity (lux; see Zipper et al., 2025 for details of data processing and units) across time, and the water presence/absence indicated by the color of each point. See *Figure S7* for sensor placement in the Appalachian Plateaus and Coastal Plain sites.

We used a project-specific data-processing pipeline to clean and quality-control STIC sensor data (Zipper et al., 2025). Briefly, for each sensor, we measured the relative conductivity in lux of DI water (0 µS/cm) as a threshold of the lowest possible wet reading to identify the transition from wet to dry relative conductivity measurements (Burke et al., 2024). We used these thresholds to convert the uncalibrated relative conductivity to a wet/dry metric (Godsey et al., 2024). For each sensor, we compared the resulting wet/dry record to field observations of water presence, and ensured that the defined thresholds yielded comparable results, manually adjusting thresholds when necessary. We quality-controlled all data by flagging any data that had negative conductivity readings or were identified as potential anomalies using a moving window z-score > 3, following Zipper et al. (2025). We removed any of these flagged observations that were obvious outliers following visual inspection, as well as any periods when no conductivity was measured. We filtered all data to periods of time where all sensors were recording concurrently to build our final dataset.

We calculated representative reach lengths for each sensor to scale our individual site observations to network extent measurements. We used the sensor GPS locations to calculate a reach length as the sum of half the distance to the downstream and upstream sensors, with the reach centered around the sensor of interest accounting for tributaries. We used these sensor measurements to calculate the extent of the active surface drainage network (ASDN, Zimmer & McGlynn, 2018) as the total length of the wet stream network in m at sub-daily and daily timesteps by summing reach lengths for all wet sensors. For each sensor, we calculated the local water persistence as the number of wet observations across the period of record divided by the total number of observations. It is worth noting that streambed sediment in the southeastern USA is highly mobile, sometimes resulting in sensor placement relative to the streambed changing through time. Similarly, our assumption that each sensor represents its neighboring 100-500 m reach might not be accurate at every time point in this study. However, comparisons between these point observations and spatially continuous mapping show that sensors usually adequately represent network-scale dynamics (Kindred et al., 2022; Figure S8).

2.2.2 Watershed Outlet Discharge Monitoring

We installed a stream monitoring well at the outlet of each watershed. The well was instrumented with a pressure transducer to measure relative stream water level (meters) at 15-min intervals throughout the duration of the study (see Plont et al., 2026). We converted the instantaneous water-level measurements to absolute elevation (meters above sea level, masl) using channel geometry surveys and a co-located pressure transducer that collected barometric pressure, and paired these data with site-specific rating curves developed using salt dilution-gauging discharge measurements to develop a record of instantaneous discharge (in L/s) at 15-min intervals.

2.3 Physiographic Analyses

We calculated a suite of metrics to characterize our networks including topographic, geologic, pedologic, and vegetative characteristics at both the site- and HGF-scales using publicly available data as well as geomorphometric tools from the *whitebox* package in R (Table S1; Wu & Brown, 2022). These metrics were selected based on previously documented drivers of network connectivity in other networks as well as local data availability. Additionally, we used field data collected in tandem with this work to calculate additional vegetative metrics at the HGF scale. All analyses were performed using R v4.4.0 (R Core Team, 2024).

We obtained high-resolution (1-m or finer) DEMs for each of our watersheds from the USGS national map downloader v2.0 (https://apps.nationalmap.gov/downloader/). We processed them by filtering, filling pits, and breaching depressions using the respective *whitebox* functions in R (Wu & Brown, 2022). We used the 'wbt_watershed()' function to delineate our watersheds, and used the d8 flow direction and flow accumulation rasters to delineate our stream networks. In the field, we observed the maximum extent of the geomorphic channel network characterized as vegetation-free areas of sediment deposition and accumulation. We defined minimum flow accumulation thresholds for each watershed that yielded networks most closely matching the geomorphic channel network (60,000 1-m cells in the Appalachian Plateaus; 10,000 0.92-m cells in the Piedmont; 12,000 1-m cells in the Coastal Plain). These watersheds and stream networks were used as the foundation for the rest of the topographic metrics.

We calculated site-specific topographic metrics at each sensor location to compare with our network metrics. We calculated elevation, slope, drainage area, distance to outlet, upstream network length, TWI, curvature, and aspect using the respective functions in the *whitebox* package (Wu & Brown, 2022), and topographic position index (TPI) by using the *multiscaleDTM* package (Ilich et al., 2025) for each sensor location (Table S1). We calculated drainage density as a proxy for topographic convergence by dividing the upstream length by the drainage area for each location. Additionally, we calculated slope in a 5-m buffer zone (buffer slope, Table S1) around each sensor by averaging all cells in the buffer to integrate riparian and valley slope conditions near the sensor. We also calculated channel slope by generating a continuous stream slope raster and averaged the slope of all cells from the stream network raster in a 12.5-m buffer that equated to a 25-m stream reach. Specifically, we identified three key topographic drivers that likely influence network dynamics: drainage density as a proxy for flow convergence, slope of the channel, and curvature (Prancevic & Kirchner, 2019).

We gathered geologic and soils data at the HGF-scale using the NRCS Web Soil Survey (Soil Survey Staff, 2025). We extracted the primary soil map units, depth to bedrock, saturated hydraulic conductivity, percentages of each soil texture class, organic matter content in the surficial 50 cm, and primary lithologic underlying units within our watersheds for each sensor location (Table S1). We aggregated these variables by HGF to evaluate relationships at a more appropriate scale, as the soil maps were developed at a coarser resolution. For each individual site, we also calculated the relative proportions of deciduous and evergreen forest in the drainage area using the National Land Cover Database for 2024 (USGS, 2024, Table S1).

2.4 Statistical Analyses

We filtered the dataset to include only non-perennial sensors (i.e., sensors that recorded dry conditions at some point across the study period; n = 13 for the Piedmont, n = 19 for the Appalachian Plateaus and Coastal Plain) for the 2024 water-year. We selected the 2024 water-year because this was the driest year of the study when all three watersheds experienced the greatest magnitude of network contraction and disconnection. Although we describe patterns across multiple years, we focus our analysis of drivers solely on the 2024 water-year for this reason. Most analyses were performed on this subset of data and were grouped by study watershed unless noted otherwise.

We accounted for our non-parametric data by performing Spearman's rank correlation tests between each variable and water persistence to evaluate the relationships between physiographic variables and water persistence. For within-watershed statistical testing, we aggregated the sensors into groups according to their HGFs (see *Section 2.1.4*). We used a Kruskal-Wallis test to evaluate significance of each physiographic variable and water persistence across the groups, though it is worth noting that the small sample sizes (n of 6 -

10 sites per group) can limit statistical power, and therefore we consider these results exploratory rather than conclusive. For significant relationships, we performed a post hoc Dunn's test to evaluate pairwise differences. For all statistical analyses, we assigned a significance level of $p < 0.05$.

We examined the relationship between stream network length and discharge using a power-law relationship and extracting the slope as our network expansion exponent (β; Figure S9; Godsey & Kirchner, 2014) to compare the variability of network extent among watersheds. To reduce noise, we aggregated our sensor-derived network extent and discharge observations to daily values by extracting paired observations at noon each day (Table S2). It is worth noting that β derived from our sensor-derived ASDN measurements should be interpreted as minimum estimates of network elasticity, as sensors can only detect water presence within the instrumented network extent and may not capture expansion into ephemeral headwater reaches during high-flow events.

3. RESULTS

3.1 Direction and magnitude of network expansion, contraction, and fragmentation varied across watersheds

Our three watersheds each had distinct spatial patterns in water persistence. In the Piedmont, only 13 sites went dry at any point ($n = 20$ total sites), which were primarily located in the headwaters of the network (Figure 2D). Nonetheless, the watershed outlet also experienced zero-flow during this period (Figure 4B), but the mainstem and lower portions of the network did not dry. In the Coastal Plain, there was a higher proportion of non-perennial sites ($n = 19$ of 20 total), but they were similarly located high in the network (Figure 2E). The only site to never go dry was in the most incised portion of the channel network. Moreover, incised regions in the middle of the network had higher water persistence than nearby un-incised reaches. In the Appalachian Plateaus, the portions of the network with the lowest water persistence were closest to the outlet, suggesting that the network contracted and dried from the bottom-up (Figure 2C). The majority of sites in the Appalachian Plateaus dried ($n = 19$ of 20 total), but the sites with the highest water persistence were clustered together in the headwaters where cave-springs have been observed in the highest density.

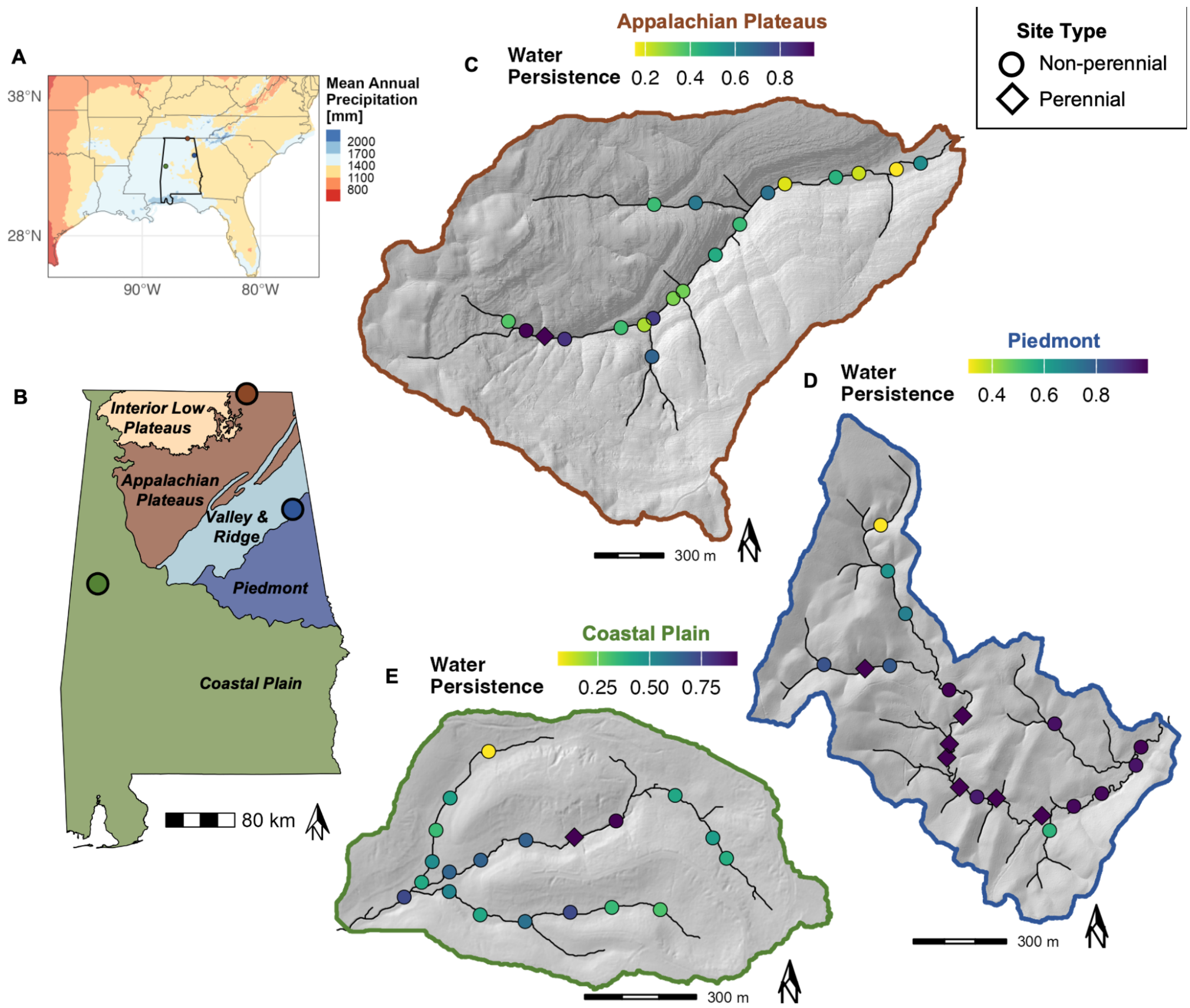

Figure 2. Research watersheds and their spatial patterns in water persistence across the 2024 water-year. (A) A map of mean annual precipitation (in mm; PRISM Group, Oregon State University, https://prism.oregonstate.edu, accessed 11 Jun 2026) across the southeastern USA, with the state of Alabama highlighted in black and individual watershed locations indicated by colored points. (B) A map of Alabama colored by physiographic provinces. Each point corresponds to one of the three research watersheds (C-E), which are also colored by physiographic province. (C-E) Hillshade maps of the three research watersheds, with the geomorphic channel network mapped by the black lines and local water persistence indicated by color. Shapes indicate perennial or non-perennial sensor types. Note: the point in (B) corresponding to the Piedmont research watershed obscures a portion of the boundary between the Valley and Ridge and Piedmont physiographic provinces; however, this watershed is entirely located in the Piedmont.

Across our three watersheds, we observed seasonal and interannual variability in network expansion, contraction, and fragmentation. In both water-years, all three watersheds exhibited greater proportions of wet sensors in late January through March as the network wetted up, and lower proportions of wet sensors in August through early November (Figure 3). However, the exact timing of the start and peak of the annual drydown varied by watershed, with the Appalachian Plateaus reaching its lowest proportion of wet sensors earlier in the water-year than the other watersheds, and the Piedmont reaching its lowest proportion of wet sensors the latest (Figure 3). Though the 2024 water-year patterns were consistent with the 2023 water-year for the Piedmont (Figure 3B), the drydown was slightly earlier in the Appalachian Plateaus (Figure 3A) and Coastal Plain (Figure 3C) for the 2024 water-year.

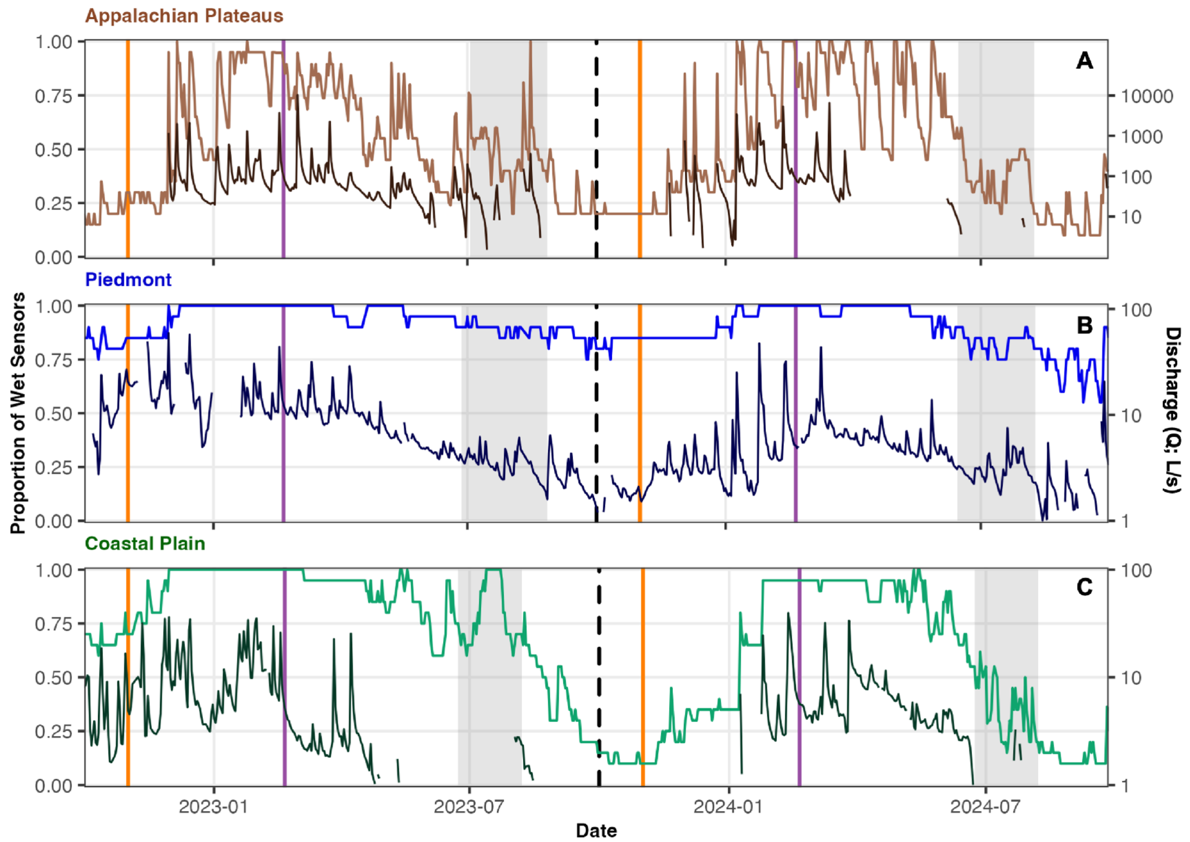

Figure 3. Daily proportion of wet sensors (lighter color) and discharge (darker color) through two water-years (where the water-year begins 1 Oct.; indicated by the black dashed line). (A) is the Appalachian Plateaus, (B) is the Piedmont, and (C) is the Coastal Plain. Periods of highest potential evapotranspiration (PET; defined as the 90th percentile of daily PET values at each site for the 2023 and 2024 water-years) for each watershed are indicated in the grey shaded area. Additionally, the start of the leaf-off period is indicated by the vertical orange dashed line (1 Nov.), and the start of the leaf-on period is indicated by the purple dashed line (20 Feb.). Leaf-on and leaf-off dates were determined based on field observations and records from the USA National Phenology Network (http://www.usanpn.org).

The magnitude of network expansion, contraction, and fragmentation differed across watersheds. The Appalachian Plateaus had a large amount of network contraction, shrinking from 100% (fully connected) in June 2024 to 10% of the sensor network wet in August 2024 (Figure 3A; ASDN ranging from 4,026 m to 238 m). This was also reflected in the expansion exponent β, which was 0.19 in the Appalachian Plateaus and indicated a relatively dynamic network. The Coastal Plain had a large magnitude of network contraction, going from 100% wet in May 2024 to 10% in August and September 2024 (Figure 3C; ASDN 2,972 m to 282 m). The β value in the Coastal Plain was 0.13, indicating a dynamic network. The Piedmont had minimal network contraction, only shrinking from 100% wet in May 2024 to 55% in September 2024 (Figure 3B; ASDN 3,326 m to 1,417 m) with a β of 0.08, suggesting a stable network. The magnitude of network contraction varied between years, with 2024 yielding lower minimum network extents for all three watersheds.

3.2 Physiographic drivers varied across watersheds

At the watershed scale, topographic metrics were variably important to water persistence across landscapes. There was a strong, negative correlation between elevation and water persistence for the Piedmont (i.e., higher elevations had lower water persistence; $\rho = -0.64$, $p < 0.01$; Table 2), but not for the Coastal Plain or Appalachian Plateaus. While some topographic metrics were correlated with water persistence for all three watersheds (e.g., TWI; Table 2), the directionality of these relationships differed between watersheds. For example, the relationship between TWI and water persistence was positive in the Piedmont ($\rho = 0.58$) and Coastal Plain ($\rho = 0.51$), but negative for the Appalachian Plateaus ($\rho = -0.53$). We found several metrics that were correlated with water persistence strongly covaried. Distance to outlet, drainage area, and TWI are all calculated using the same area-accumulation technique, and TWI was correlated with water persistence across all three watersheds. Altogether, we expect that the relationships observed here likely reflect larger-scale watershed patterns, and thus may correlate with other physiographic drivers.

Table 2. Spearman's Correlation Coefficients (ρ) and Statistical Significance for All Topographic Metrics

Water Persistence ~	**Appalachian Plateaus**		**Piedmont**		**Coastal Plain**	
	ρ	***p*-value**	**ρ**	***p*-value**	**ρ**	***p*-value**
Drainage density	*0.09*	*0.13*	***0.60***	*0.22*	*0.52*	*0.06*
Channel Slope	*0.49*	***0.01***	***-0.65***	***< 0.01***	*-0.25*	*0.45*
Curvature	*0.21*	*0.63*	*-0.48*	***0.05***	*0.46*	***< 0.01***
Elevation	0.41	0.06	**-0.64**	**< 0.01**	-0.39	0.13
Slope	0.54	0.06	**-0.63**	**< 0.01**	0.25	0.44
Buffer slope	0.52	**0.04**	**-0.61**	**0.02**	**0.64**	**< 0.01**
Distance to outlet	0.36	0.06	**-0.67**	**0.02**	-0.24	0.39
Drainage area	-0.37	0.07	**0.71**	**0.01**	**0.72**	**< 0.01**
TWI	-0.53	**0.03**	0.58	**< 0.01**	0.51	**0.02**
TPI	0.09	0.61	0.32	0.20	-0.49	**< 0.01**

Note: All statistics performed on the non-perennial sensors (Piedmont $n = 13$, Appalachian Plateaus and Coastal Plain $n = 19$). Variables in bold are strongly correlated ($\rho > 0.6$) or statistically significant ($p < 0.05$). The three italicized variables are proxies for the three key topographic variables (see *Section 2.3*).

We did not observe consistent patterns between water persistence and the three key topographic metrics that have been previously linked to network dynamics. Drainage density was only correlated with water persistence in the Piedmont ($\rho = 0.60$; $p = 0.22$), but this relationship was not significant in any watershed (Figure 4A, Table 2). Channel slope was correlated to water persistence in the Appalachian Plateaus ($\rho = 0.49$, $p = 0.01$) and the Piedmont ($\rho = -0.65$, $p < 0.01$; Table 2), but with opposite signs. The relationship was positive in the Appalachian Plateaus where steeper slopes related to greater water persistence, but negative in the Piedmont where shallower slopes related to greater water persistence (Figure 4B). Greater curvature led to higher water persistence in the Coastal Plain ($\rho = 0.46$,

$p < 0.01$; Figure 4C, Table 2), but lower water persistence in the Piedmont (ρ = -0.48, p = 0.05; Figure 4C, Table 2). Altogether, water persistence in each watershed was correlated to at least one, but not all three, of the key topographic variables, with no single variable being correlated with water persistence in all three watersheds.

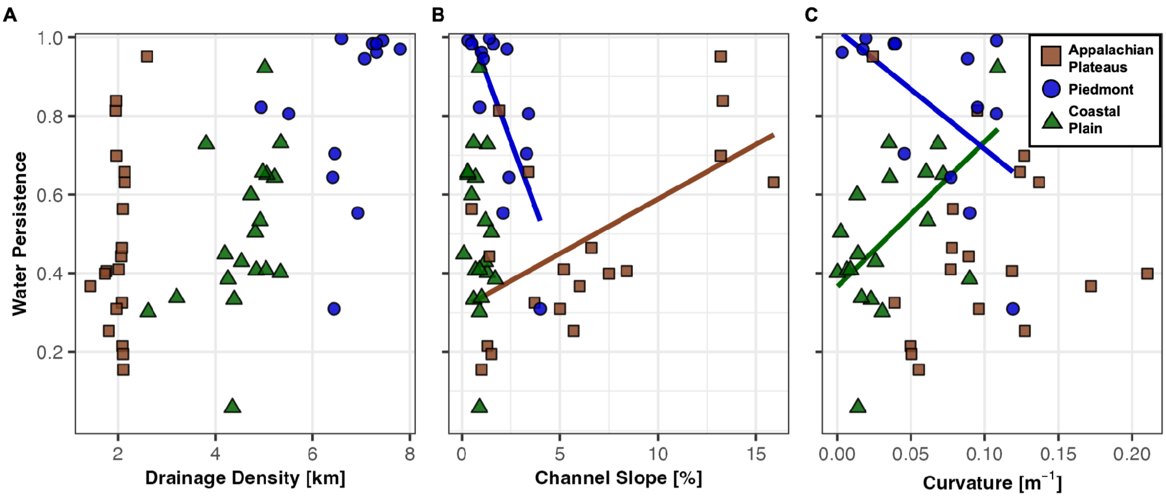

Figure 4. Relationships between site-specific annual water persistence and the three key topography metrics: (A) drainage density as a proxy for flow convergence, (B) slope of the channel, and (C) curvature. Relationships with significant correlations (as noted in Table 2) are marked with solid lines. Colored points and lines correspond to the watersheds in this study, where brown is the Appalachian Plateaus, blue is the Piedmont, and green is the Coastal Plain (further indicated in the legend).

At the HGF scale, we observed within-watershed patterns in water persistence that aligned with within-watershed geologic, vegetative, and soil characteristics (Table S1). In the Appalachian Plateaus, the downstream A2 HGF dried 16% more than A1, although this difference was not significant (p = 0.14; Figure 5A). There were significant differences in depth to bedrock (p = 0.03; Figure 5D) and all other soil variables between the two Appalachian Plateaus HGFs (Table S3). In the Piedmont, the most-upstream HGF (P1) was 28% drier than the P2 HGF on average (p = 0.05; Figure 5B), but there were no significant differences between other HGFs. This was also reflected in the physiographic variables, where the P1 HGF had shallower depths to bedrock ($p < 0.01$), higher saturated hydraulic conductivities ($p < 0.01$), and greater percentages of coniferous vegetation ($p < 0.01$; Figure 5E; Table S3). In the Coastal Plain, the C1 and C2 HGFs were approximately 23% drier than the most-downstream and incised HGF (C3; p = 0.03, Figure 5C). There were no significant relationships between HGF and physiographic variables in this watershed (Table S3), which we attribute to the unequal distribution of sites in each HGF.

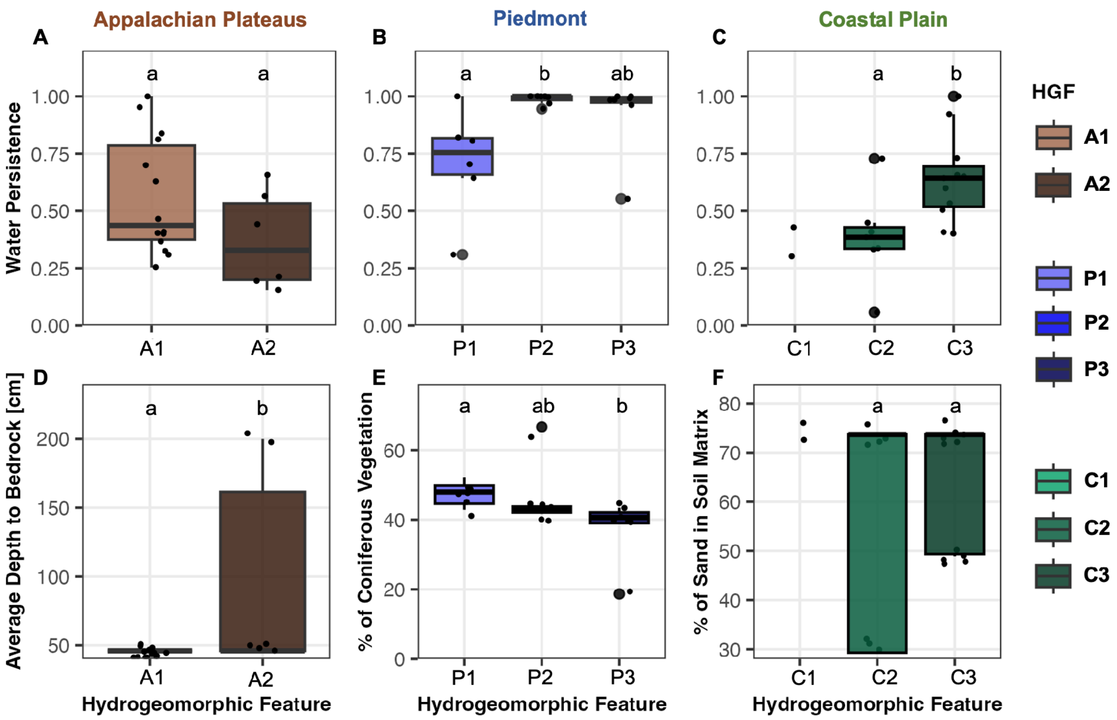

Figure 5. (A-C) Boxplots of water persistence across the HGFs for each watershed. (D-F) Plots of variables from all physiographic categories across the HGFs for each watershed. Significant differences between groups are denoted by letters above each group ($p < 0.05$). Analyses were performed on the entire dataset ($n = 20$ per watershed rather than the subsetted non-perennial data) for a more even distribution across groups, and groups with less than 6 sites were excluded from analyses. HGFs are ordered from most upstream to downstream. Panels (D-F) show variables from different physiographic categories: (D) depth to bedrock as a proxy for geologic features, (E) percent coniferous vegetation as a proxy for vegetative community structure, and (F) percentage of sand in the soil matrix as a proxy for soil structure.

3.3 Sensor placement influenced the results of network-scale expansion, contraction, and fragmentation

There were key differences in the magnitude of network expansion, contraction, and fragmentation when the more extensive sensor network was deployed in the Piedmont from May 2022 through April 2023. Using only the 20 permanent sensors to assess network state in the Piedmont, the network appeared highly stable in the 2023 water-year, with a maximum and minimum extent of 3,330 m and 2,540 m respectively. However, when ASDN was calculated using the high-density sensor network that extended further into the upstream tips of the geomorphic channel network, the Piedmont stream network was more dynamic and expanded to 5,320 m during precipitation events before contracting to 2,740 m during drydown (Figure 6A). Together, these results show that both sensor networks captured similar network extents during the drydown, but the high-density network better captured expansion in the ephemeral headwater reaches of the network during precipitation events.

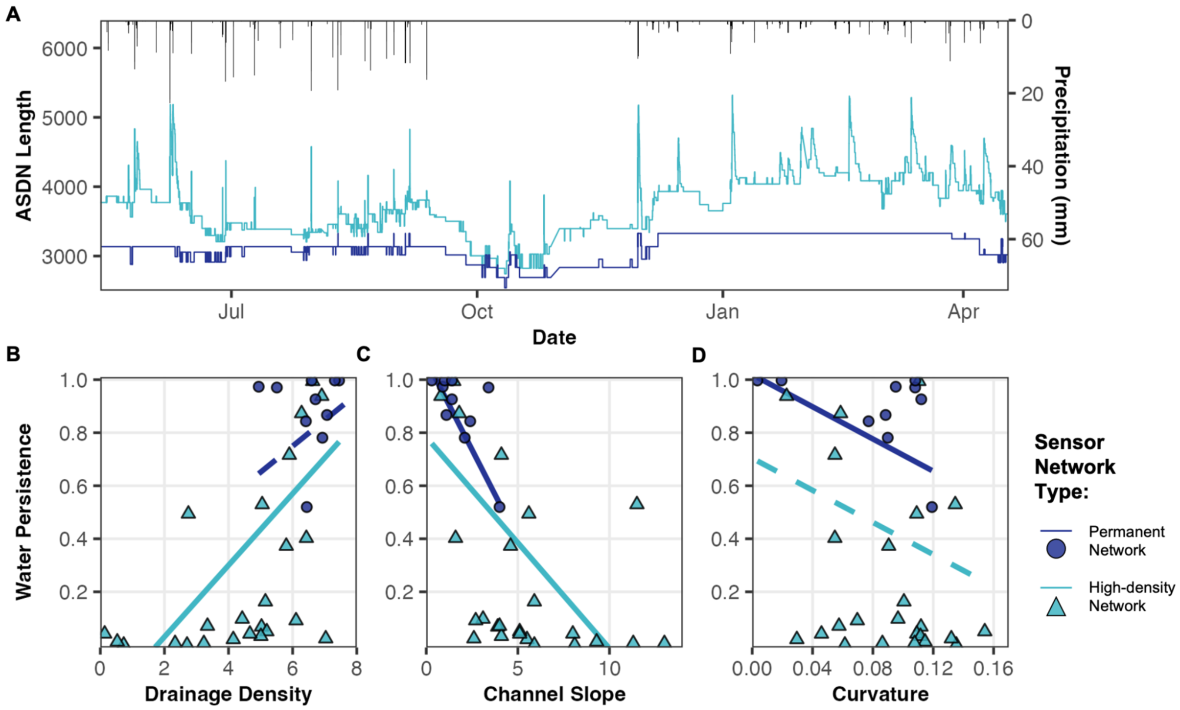

Figure 6. (A) ASDN for the Piedmont research watershed as calculated from the permanent (n = 20) sensors in dark blue and from the high-density network (n = 49) in light blue, with concurrent precipitation totals in black. (B-D) scatterplots of the relationships between the three key topographic metrics and the water persistence of all non-perennial STICs for this time period (n = 34 total; n = 10 in the permanent network, n = 24 in the high-density network). Correlations are colored by the network type, and solid lines indicate a significant ($p < 0.05$) relationship, where dashed lines indicate nonsignificance.

We compared the relationships between the key topographic drivers and site-specific water persistence using the high-density network. When considering the permanent network, there were significant relationships between water persistence for both slope and curvature (Table 2; Figure 6C-D). In the high-density network, while slope was also negatively correlated to water persistence (ρ = -0.79, $p < 0.01$), there was no correlation between curvature and water persistence (ρ = -0.25, p = 0.13; Figure 6D). In the high-density network, there was a positive relationship between drainage density and water persistence (ρ = 0.73, $p < 0.01$; Figure 6B) where there was no correlation in the permanent network (Table 2). Together, these results highlight the variability in topographic drivers of network expansion, contraction, and fragmentation across scales.

4. DISCUSSION

We examined network-scale expansion, contraction, and fragmentation, as well as the drivers of water persistence across three physiographic provinces that experience similar precipitation patterns. This allowed us to investigate the impacts of topography, geology, and vegetation on network dynamics without the confounding influence of precipitation – which is generally considered the primary control on streamflow and network extent. Moreover, our study focused on low-relief systems, which are underrepresented in contemporary studies of network dynamics. Here, we first investigated the interactions between physiographic variables and watershed-scale connectivity to link potential landscape drivers to network dynamics. Next, we specifically explored the relationships between key topographic variables and network expansion, contraction, and fragmentation within watersheds. Finally, we discuss the influence of spatial scale on observations within our watersheds.

4.1 Watershed-scale patterns in connectivity are driven by interactions between topographic, geologic, and biotic variables

Hierarchical drivers are hypothesized to interact predictably across subordinate scales to drive emergent patterns of streamflow generation and network connectivity (McDonnell et al., 2007). At large spatial scales, there is general agreement that observable network-scale patterns in connectivity reflect and integrate hydroclimatic, geologic, and biologic conditions across both spatial and temporal scales (e.g., Godsey & Kirchner, 2014; Newcomb & Godsey, 2023; Ward et al., 2018). Further, it has been well documented that variability in these conditions across space translates to watershed-scale variability in network connectivity (e.g., Jensen et al., 2017; Lovill et al., 2018). However, we do not yet have a clear and predictive understanding of the drivers of network variability – and the interactions among them – across landscapes. For example, Hewlett & Hibbert (1967) observed that in a high-relief watershed in the Appalachian mountains, streamflow generation was controlled primarily by depth to an impervious layer, followed hierarchically by topography, climate, and land use. Other studies have documented meteorology and land use or land cover as key first-order controls on network connectivity across regions (Costigan et al., 2016; Hammond et al., 2021; Zipper et al., 2021). Therefore, identifying the primary watershed-scale controls on network dynamics is challenging and often site-specific.

In this study, there was consistent climate and land use across our study watersheds, yet we still observed significant differences in network connectivity (Figure 3; similar to the findings in Lovill et al., 2018). Therefore, these observed patterns must be due to other controls, which we expect may be differences in physiographic variables across these regions. Physiography is generally defined as the geologic, topographic, and biotic features of the landscape (Fenneman, 1938), thereby integrating multiple potential drivers of network expansion, contraction, and fragmentation to provide a more holistic view of watershed settings. In this vein, our results highlight significant relationships between water persistence and a combination of soil, vegetation, and topographic characteristics in every watershed (Table 2, Figure 5), suggesting that physiography provides a useful template for evaluating hydrologic patterns.

4.1.1 Topographic variables

While topography plays a large role in how water moves through watersheds (see *Section 4.2*), our data highlight the importance of considering other aspects of physiography across watersheds. For example, in the low relief of the Coastal Plain, our results paired with other studies suggest that where there are minimal slope changes that would normally drive flow to the surface, topographic convergence will instead drive flow generation (Montgomery & Dietrich, 1995). Additionally, the positive relationship between curvature and water persistence in the Coastal Plain likely reflects erosive and compressive processes that reduce down-valley flows and increase water persistence (Prancevic & Kirchner, 2019). Many studies have attributed this pattern in curvature and transmissivity to bedrock fracturing and weathering processes (e.g., Miller & Dunne, 1996; Moon et al., 2017). However, in our low-relief Coastal Plain watershed where bedrock is tens of meters deep, this pattern likely reflects the importance of stream incision and channel erosion in dictating flow generation and persistence (Peterson et al., 2025). Figure 5C highlights that the highest water persistence values are found in the HGF characterized by channel incision, which can increase lateral connectivity from riparian water tables to the stream channel and potentially sustain flows (Peterson et al., 2025; Kirker at al., 2025). Further, we anticipate that the relationship between slope and water persistence in the Piedmont reflects a decrease in slope that slows subsurface valley flow, resulting in subsurface water being forced to the surface (Prancevic et al., 2025). Together, our research watersheds demonstrate alternative ways that topographic variables can influence network extent and connectivity.

4.1.2 Geologic variables

Our results also demonstrate the role underlying geology and resulting soil characteristics play in network connectivity. In the Appalachian Plateaus, reaches in the most upstream HGF were generally wetter than reaches in the downstream HGF (Figure 2C, Figure 5A). In the uppermost HGF, a combination of karst geologic formations and shallow soils likely explains increased flow persistence. These reaches are located in the outcropping of the Bangor limestone unit, which contains a high density of caves and karst formations (Ponta, 2018) that are likely persistent sources of deep groundwater (Hartmann et al., 2014; see *Section 4.2*). Moreover, reaches in the upstream HGF had shallow soils (Figure 5D) and thus lower capacity for subsurface flow. In contrast, reaches in the valley bottom HGF experienced decreased flow persistence likely due to increased subsurface storage in alluvial deposits. As the valley transitioned to lower-gradient reaches dominated by alluvial deposits and increased subsurface storage (Figure 5D), subsurface capacity to transmit flow drastically increased, likely resulting in observed stream drying. Other studies have documented similar disconnectivities occurring within networks as a result of heterogeneity in subsurface architecture (Glaser et al., 2025; Jensen et al., 2017; Whiting & Godsey, 2016), further reinforcing the role both geology and soil structure play within networks. These results are further supported by our observations in the Piedmont watershed, where the drier headwaters also had shallower depths to bedrock and higher saturated hydraulic conductivities with coarser soil textures. These soil conditions likely increased transmissivity, which contributes to lower water persistence as water is moved down-valley more efficiently (Godsey & Kirchner, 2014). Together, these two watersheds highlight the role geologic setting plays in driving network connectivity.

4.1.3 Vegetative variables

Our findings suggest that vegetative communities can contribute both spatially and temporally to network-scale patterns in connectivity. As all three research watersheds were forested, we interpret the timing of network contraction in the late summer and early autumn to be a function of vegetative water demand and transpiration during the peak growing season (Figure 3). The timing of network reconnection and expansion in the late autumn and early winter coincides with leaf-off and vegetative dormancy, which reduces vegetative water demand (Figure 3). For example, Bergstrom et al. (2025) observed that the timing and likelihood of stream drying was tied to seasonal climatic patterns like temperature, which when paired with water availability drives ET. Taken with our results, these dynamics highlight that the timing of network drying in our watersheds is closely linked with the timing of plant productivity and water use.

Additionally, we observed notable spatial patterns in forest composition within our watersheds. For example, the distribution of coniferous and deciduous species of the Piedmont watershed mirrored patterns in water persistence, in that there was more coniferous vegetation in the drier headwaters. The coniferous vegetation could result in both more consistent vegetative water demand throughout the year (Swank et al., 1989; Young-Robertson et al., 2016) and increases in interception that decrease infiltration and soil-water recharge (Rutter at al., 1975). However, there are complex feedbacks between plant water use and water availability for streamflow (Bergstrom et al., 2025); for example, many coniferous species require well-drained, drier soils like those found in the headwaters of the Piedmont. Taken together, the network connectivity in the Piedmont watershed is likely a function of feedbacks in vegetative water demand, where the headwaters were increasingly drier as plant-water interactions reduced subsurface water storage. This aligns with other studies that found vegetative patterns influence connectivity at reach (Newcomb & Godsey, 2023, Warix et al., 2021) and network scales (Lee et al., 2020; Bergstrom et al., 2016). Altogether, the topographic, geologic, and vegetative context of these watersheds explains the observed patterns within our networks better than topography alone.

4.2 Relationships between topography and network expansion, contraction, and fragmentation varied across and within our study watersheds in unexpected ways

While many studies have investigated the role topography plays in regulating network expansion and contraction, recent analysis across watersheds suggests that channel convergence, slope, and valley curvature are key drivers of network dynamics. However, these three variables were not consistently correlated with water persistence in our study (Figure 4). While channel slope was correlated with water persistence for both the Piedmont and Appalachian Plateaus, the relationship was positive in the Appalachian Plateaus and negative in the Piedmont. Previous studies documented a negative relationship between channel slope and water persistence like the one observed in the Piedmont, where decreasing slope decreases subsurface flow and drives water to the surface to create higher water persistence (Montgomery & Dietrich, 1995; Rinderer et al., 2014; Prancevic & Kirchner, 2019). The Appalachian Plateaus demonstrated the opposite pattern, in which steeper slopes were correlated with locations of increased water persistence (see *Section 4.1*). While this is not the first study to find that topography does not fully explain network variability (e.g., Warix et al., 2021; Whiting & Godsey, 2016), our results show that our watersheds do not always align with these expected patterns, likely due to interactions between other controls such as soil structure, underlying geology, and vegetative water demand (Figure 5).

We found a similar pattern for curvature in the Coastal Plain and Piedmont watersheds. While valley curvature was related to water persistence in both watersheds, it was positively correlated in the Coastal Plain, and negatively correlated in the Piedmont. This also contradicts expectations; presuming that curvature is a proxy for valley transmissivity as a function of subsurface area and compressive forces (Prancevic & Kirchner 2019), we would expect higher curvature to relate to higher water persistence. Therefore, the Coastal Plain aligned with these expectations and is consistent with other studies (e.g., Kaplan et al., 2020). However, the Piedmont demonstrated the opposite pattern, where greater curvatures were related to locations of lower water persistence, which to our knowledge has not been documented in other networks. However, other studies have found curvature to be an overall poor predictor of water persistence (Warix et al., 2021), suggesting complex interactions between valley curvature and streamflow permanence.

We also observed similar dynamics for TWI, which was one of the only significant metrics across all three watersheds. We observed the expected positive correlation between water persistence and TWI for both the Piedmont and the Coastal Plain, where higher TWIs were related to higher persistence portions of the network. However, the Appalachian Plateaus watershed demonstrated the opposite pattern, where portions of the network with higher TWIs had lower water persistence than other portions of the network. Given that TWI integrates both drainage area and slope (Beven & Kirkby, 1979), the Appalachian Plateaus watershed contradicts the assumption that larger areas paired with lower slopes yield wetter conditions. We anticipate these unexpected patterns in topographic variables are more an expression of the bottom-up drying pattern we observed at this site (Figure 2C). While the standard conceptualization is that networks expand and contract from the top-down (Biswal & Marani, 2010), our Appalachian Plateaus watershed disconnected at the outlet before contracting up-network, which has only been documented in a handful of other studies, often in more arid regions (e.g., Costigan et al., 2015; Senatore et al., 2021; Zipper et al., 2025). We expect these patterns are primarily caused by the geologic setting; the Appalachian Plateaus is karst, and the majority of cave-springs and resulting locations of greatest water persistence were located in the headwaters of this network, where contributing areas are small and slopes are steep. The influence of lithologic complexity on water persistence is widely acknowledged; heterogeneity in subsurface architecture like that found in karst landscapes often introduces springs that can sustain streamflow and localized high water persistence, potentially overpowering other physiographic controls (e.g., Zipper at al., 2025; Senatore et al., 2021; Crowther et al., 2026). Taken together, the varying importance of topography across these sites points to the importance of considering other landscape-level drivers in low-relief networks; in the absence of clear topographic controls, the heterogeneity of otherwise subordinate controls like geology and vegetation can be more significant predictors of hydrologic dynamics.

4.3 Within-watershed patterns in connectivity are tied to the scales of observation

Despite our standardized site design, we found that placement of sensors affected our network-scale results. Generally, emergent watershed properties are based on the scales of observation, and so the patterns observed at one scale integrate all processes occurring at subordinate scales (McDonnell et al., 2007). Therefore, based on the established relationship between area accumulation and streamflow generation (e.g., Beven & Kirkby, 1979), we expected stream heads to occur at similar thresholds in similarly sized watersheds with consistent precipitation inputs (Montgomery & Dietrich, 1989). However, the results in our Coastal Plain and Piedmont watersheds did not demonstrate this, with the transition from non-perennial to perennial flow occurring much higher in the network in the Piedmont than the Coastal Plain (Figure 2D-E). We expect that this is likely a function of the geologic setting of these watersheds; given the shallow and likely fractured bedrock of the Piedmont watershed, deep groundwater from fracture-flow likely contributed to streamflow in its headwaters (Boutt et al., 2010). This would generate more perennial flow higher in the network compared to the Coastal Plain, where flow persistence is likely driven by topographic convergence, soil properties, and channel incision (Gutiérrez-Jurado et al., 2019; Montgomery & Dietrich, 1995; Peterson et al., 2025).

Our results in the Piedmont emphasize the importance of site selection and sensor distribution on network-scale patterns. We found that better capturing the non-perennial portions of our

Piedmont network strengthened the relationships between water persistence and topographic metrics. However, of the three key topographic metrics (drainage density, channel slope, and curvature; Prancevic & Kirchner, 2019), only drainage density and channel slope were statistically significant predictors of water persistence in the permanent network (n = 20). Conversely, channel slope and curvature were the only significant predictors of water persistence in the high-density network (n = 49). Therefore, while the significance of channel slope on water persistence increased with the higher density network, this was the only topographic metric that was significant in both sensor networks. Moreover, the high-density network captured a larger magnitude of network expansion, contraction, and fragmentation, though this only marginally affected the generally low observed β (Figure S10). However, it is worth noting that our definition of connectivity integrates disconnectivity (Glaser et al., 2025) into this expansion and contraction framework, meaning that network expansion corresponds to an increase in total network extent rather than contiguous flow. Therefore, our results represent an initial attempt at characterizing the flow dynamics of small, flashy, low-relief systems, but future work could further investigate the reach-scale dynamics in flow that are not captured as effectively by our sensor networks.

We originally placed the permanent sensors in the Piedmont watershed based on the relationship between area accumulation and slope (Zipper et al., 2025). Without prior knowledge of the true dynamics of the system, our sensor placement strategy resulted in a bias towards lower, wetter portions of the network. While there is a precedent for distributing sensors randomly or evenly throughout a network to better capture a range of conditions (e.g., Jaeger & Olden, 2012; Jensen et al., 2019; Warix et al., 2021), this approach was less effective in our Piedmont watershed – likely due to the relatively small area accumulation thresholds. However, if our sensor design had been able to account for the potential for fracture flow to occur higher in the network, we could have distributed the sensors across a more representative gradient of wetness conditions. Therefore, our study highlights the importance of considering more than just topographic conditions when designing and deploying sensor networks.

4.4 Methodological limitations and future research directions

There are inherent challenges to capturing variability in network extent within flashy systems, where network extent can change substantially within minutes to hours. Here, we employed a dense network of water presence/absence sensors in an effort to capture this variability, which necessitated making assumptions about conditions between sensors. In particular, the β values reported here should be interpreted cautiously when compared to β values calculated from stream-walking (Godsey and Kirchner, 2014) or hydrologic modelling studies (Mahoney et al., 2023), as all three methods have methodological limitations. Sensor-based estimates of β likely compress length-discharge relationships due to the censored nature of the network extent measurements at high flows. Stream-walking primarily characterizes network extent at baseflow due to logistical constraints, especially in flashy networks like those studied here. Most modelling studies rely on *a priori* definitions of maximum network extent and simplified representations of surface water and groundwater exchange flows. Therefore, further work is needed to better understand the comparability of these three approaches to characterizing network dynamics.

Our results highlight the importance of balancing both unbiased sensor distributions with an understanding of the dynamics of the study system. It can be challenging to find an appropriate balance in previously unstudied locations and in systems that are underrepresented in our perceptual models (e.g., low-relief watersheds). With that in mind, we suggest that future studies continue to integrate both empirical observations of network length with systematic sensor deployment strategies. Here, we used the topographically-based stratified distribution (Figure 1A) as an initial attempt to build a perceptual model of our systems. We then used our observations of network extent dynamics and the geomorphic channel from the first year of data collection to update our understanding of the system, and distribute our high-density network to collect additional data in more dynamic portions of the network. Many other studies have used empirical observations of network extent at high spatial and lower temporal resolution (stream-walking; Whiting & Godsey, 2016, Durighetto et al., 2020). Other studies have used sensor networks to measure both water persistence and network-scale patterns at high temporal and lower spatial resolution (e.g., Zanetti et al., 2022). Studies that have used both stream-walking and sensor networks are limited, but suggest that patterns observed with sensor networks are representative of even highly-dynamic networks (Jensen et al. 2019, Kindred, 2022). Altogether, we emphasize that there are tradeoffs and considerations related to empirical data collection in dynamic networks, and consideration of the spatial and temporal scales of interest should drive sensor network design and data collection efforts. We suggest future work focuses on both the integration of techniques and the collection of data in diverse landscapes to better inform our understanding of network patterns across study systems.

5. CONCLUSIONS

We used a high-resolution sensor network to measure network connectivity in three watersheds spanning the physiographic regions of the southeastern USA. We used both empirical and geospatial data to explore potential drivers of network expansion across landscapes, and compared these results at both the watershed and site scales to identify key patterns in network connectivity. Our study found that network dynamics in low-relief systems in the southeastern USA were best reflected by a combination of topographic, geologic, and vegetative variables. When comparing three key topographic drivers – drainage density as a proxy for flow convergence, slope, and valley curvature – we found that no single driver explained the variability observed in all three watersheds; furthermore, no watershed had a significant relationship with all three topographic drivers. However, by integrating physiographic drivers like soil properties, geology, and plant communities, we could better explain the network patterns observed. Additionally, we found that the placement and number of sensors influenced the significance of topographic drivers.

Altogether, our study demonstrates that physiography is a useful framework and potential starting point for developing predictive relationships between watershed characteristics and hydrologic processes. While this work is limited to three watersheds, it is an initial characterization of network expansion, contraction, and fragmentation in low-relief systems, which are underrepresented in our perceptual models of network dynamics. Further, these findings also highlight that low-relief network dynamics can be driven by complex interactions between physiographic characteristics, and contradict patterns observed in other landscapes. These results help build a more holistic picture of the patterns and processes of network expansion, contraction, and fragmentation across landscapes, which is important as non-perennial streams provide critical physical, chemical, and biological functions to downstream waterways. Moreover, as climate change potentially increases stream intermittency in regions like the southeastern USA, these initial characterizations can provide additional context and predictability to changing network dynamics in this region.

ACKNOWLEDGEMENTS

The authors received support from the AIMS Project (funded by the National Science Foundation, Award Number 2019603), the University of Alabama Graduate School, and the Alabama Water Institute. The authors would like to thank the US Forest Service, the Weyerhaeuser Company, and private landowner John Gully for their management and support of the research watersheds. The authors would also like to thank Jami Nettles, Ashleigh Kirker, Helen Czech, Patience Knight, Lidia Molina Serpas, Justus King, Caroline Anscombe, Jacob Ackerman, Kevin Shaw, Jasmine Morejon, Stella Wilson, Vanessa Marshall, and many other friends and colleagues for their help with instrument maintenance, site management, and fieldwork. We thank Steve Wondzell for his helpful feedback and suggestions to improve this manuscript. We also gratefully acknowledge Dana Lapides and two other anonymous reviewers for time and effort in providing valuable feedback. We also thank Jeff Prancevic for his help and engagement with earlier versions of this manuscript. The authors declare no conflicts of interest relevant to this study.

DATA AVAILABILITY

All data used in this study are available through CUAHSI HydroShare in the public AIMS Data group (https://www.hydroshare.org/group/247), and are linked in the references below. Additional information about these and co-collected data can be found in Plont et al. (2026; https://doi.org/10.5194/essd-2025-559). Associated analyses and scripts can be accessed at: https://github.com/dmpeterson2/STIC_physiographic_analyses#

REFERENCES

Bergstrom, A., Jencso, K., & McGlynn, B. (2016). Spatiotemporal processes that contribute to hydrologic exchange between hillslopes, valley bottoms, and streams. Water Resources Research, 52(6), 4628–4645. https://doi.org/10.1002/2015WR017972

Bergstrom, A., Price, A. N., Beers, M., & Roche, K. R. (2025). Climate Forcings Across Multiple Timescales Control Stream Drying and Wetting in a Headwater Catchment. Hydrological Processes, 39(6), e70167. https://doi.org/10.1002/hyp.70167

Bernal, S., Lupon, A., Wollheim, W. M., Sabater, F., Poblador, S., & Martí, E. (2019). Supply, Demand, and In-Stream Retention of Dissolved Organic Carbon and Nitrate

During Storms in Mediterranean Forested Headwater Streams. Frontiers in Environmental Science, 7. https://doi.org/10.3389/fenvs.2019.00060

Beven, K. J., & Kirkby, M. J. (1979). A physically based, variable contributing area model of basin hydrology / Un modèle à base physique de zone d'appel variable de l'hydrologie du bassin versant. Hydrological Sciences Bulletin, 24(1), 43–69. https://doi.org/10.1080/02626667909491834

Biswal, B., & Marani, M. (2010). Geomorphological origin of recession curves. Geophysical Research Letters, 37(24). https://doi.org/10.1029/2010GL045415

Botter, G., & Durighetto, N. (2020). The Stream Length Duration Curve: A Tool for Characterizing the Time Variability of the Flowing Stream Length. Water Resources Research, 56. https://doi.org/10.1029/2020WR027282

Boutt, D. F., Diggins, P., & Mabee, S. (2010). A field study (Massachusetts, USA) of the factors controlling the depth of groundwater flow systems in crystalline fractured-rock terrain. Hydrogeology Journal, 18(8), 1839–1854. https://doi.org/10.1007/s10040-010-0640-y

Brinkerhoff, C. B., Gleason, C. J., Kotchen, M. J., Kysar, D. A., & Raymond, P. A. (2024). Ephemeral stream water contributions to United States drainage networks. Science, 384(6703), 1476–1482. https://doi.org/10.1126/science.adg9430

Burke, E., Wilhelm, J., Zipper, S., & Brown, C. (2024). AIMS SOP STIC Calibration. CUAHSI HydroShare. Retrieved from https://hydroshare.org/resource/9f2027c779d64149be32bdb9eede54f2/

Burt, T. P., & McDonnell, J. J. (2015). Whither field hydrology? The need for discovery science and outrageous hydrological hypotheses. Water Resources Research, 51(8), 5919–5928. https://doi.org/10.1002/2014WR016839

Busch, M. H., Costigan, K. H., Fritz, K. M., Datry, T., Krabbenhoft, C. A., Hammond, J. C., et al. (2020). What's in a Name? Patterns, Trends, and Suggestions for Defining Non-Perennial Rivers and Streams. Water, 12(7), 1980. https://doi.org/10.3390/w12071980

Chapin, T. P., Todd, A. S., & Zeigler, M. P. (2014). Robust, low-cost data loggers for stream temperature, flow intermittency, and relative conductivity monitoring. Water Resources Research, 50(8), 6542–6548. https://doi.org/10.1002/2013WR015158

Costigan, K. H., Daniels, M. D., & Dodds, W. K. (2015). Fundamental spatial and temporal disconnections in the hydrology of an intermittent prairie headwater network. Journal of Hydrology, 522, 305–316. https://doi.org/10.1016/j.jhydrol.2014.12.031

Costigan, K. H., Jaeger, K. L., Goss, C. W., Fritz, K. M., & Goebel, P. C. (2016). Understanding controls on flow permanence in intermittent rivers to aid ecological research: integrating meteorology, geology and land cover. Ecohydrology, 9(7), 1141–1153. https://doi.org/10.1002/eco.1712

Crowther, E., McNamara, J. P., Godsey, S. E., Bergstrom, A., & Kaiser, K. E. (2026). Springs Impact Active Stream Lengths and Stream Permanence. Hydrological Processes, 40(6), e70597. https://doi.org/10.1002/hyp.70597

Czikowsky, M. J., & Fitzjarrald, D. R. (2004). Evidence of Seasonal Changes in Evapotranspiration in Eastern U.S. Hydrological Records. Retrieved from https://journals.ametsoc.org/view/journals/hydr/5/5/1525-7541_2004_005_0974_eoscie_2_0_co_2.xml

Datry, T., Boulton, A. J., Bonada, N., Fritz, K., Leigh, C., Sauquet, E., et al. (2018). Flow intermittence and ecosystem services in rivers of the Anthropocene. The Journal of Applied Ecology, 55(1), 353–364. https://doi.org/10.1111/1365-2664.12941

Durighetto, N., Vingiani, F., Bertassello, L. E., Camporese, M., & Botter, G. (2020). Intraseasonal Drainage Network Dynamics in a Headwater Catchment of the Italian Alps. Water Resources Research, 56(4), e2019WR025563. https://doi.org/10.1029/2019WR025563

Feminella, J. W. (1996). Comparison of Benthic Macroinvertebrate Assemblages in Small Streams along a Gradient of Flow Permanence. Journal of the North American Benthological Society, 15(4), 651–669. https://doi.org/10.2307/1467814

Fenneman, N. M. (1938). Physiography of eastern United States. McGraw-Hill Book Company, inc. Retrieved from http://archive.org/details/physiographyofea0000nevi

Glaser, C., Gannon, J. P., Godsey, S. E., Grande, E., & Klaus, J. (2025). Streamflow (De)generation—How Do Streams Lose Flow? Hydrological Processes, 39(10), e70258. https://doi.org/10.1002/hyp.70258

Godsey, S., Wheeler, C., & Zipper, S. (2024). AIMS SOP STIC Deployment and Maintenance | CUAHSI HydroShare. CUAHSI HydroShare. Retrieved from https://hydroshare.org/resource/c82a87a6c63445029d35131260241386/

Godsey, S. E., & Kirchner, J. W. (2014). Dynamic, discontinuous stream networks: hydrologically driven variations in active drainage density, flowing channels and stream order. Hydrological Processes, 28(23), 5791–5803. https://doi.org/10.1002/hyp.10310

Gómez-Gener, L., Siebers, A. R., Arce, M. I., Arnon, S., Bernal, S., Bolpagni, R., et al. (2021). Towards an improved understanding of biogeochemical processes across surface-groundwater interactions in intermittent rivers and ephemeral streams. Earth-Science Reviews, 220, 103724. https://doi.org/10.1016/j.earscirev.2021.103724

Gutiérrez-Jurado, K. Y., Partington, D., Batelaan, O., Cook, P., & Shanafield, M. (2019). What Triggers Streamflow for Intermittent Rivers and Ephemeral Streams in Low-Gradient Catchments in Mediterranean Climates. Water Resources Research, 55(11), 9926–9946. https://doi.org/10.1029/2019WR025041

Hammond, J. C., Zimmer, M., Shanafield, M., Kaiser, K., Godsey, S. E., Mims, M. C., et al. (2021). Spatial patterns and drivers of non-perennial flow regimes in the contiguous U.S. Geophysical Research Letters, n/a(n/a), 2020GL090794. https://doi.org/10.1029/2020GL090794

Hartmann, A., Goldscheider, N., Wagener, T., Lange, J., & Weiler, M. (2014). Karst water resources in a changing world: Review of hydrological modeling approaches. Reviews of Geophysics, 52(3), 218–242. https://doi.org/10.1002/2013RG000443

Harvey, J., & Gooseff, M. (2015). River corridor science: Hydrologic exchange and ecological consequences from bedforms to basins. Water Resources Research, 51(9), 6893–6922. https://doi.org/10.1002/2015WR017617

Hewlett, J., & Hibbert, A. (1967). Factors Affecting the Response of Small Watersheds to Precipitation in Humid Areas. In Proceedings of the International Symposium on Forest Hydrology. Pergamon, Pennsylvania State University, NY.

Hupp, C. (2000). Hydrology, Geomorphology and Vegetation of Coastal Plain Rivers in the South-Eastern USA. Hydrological Sciences, 14, 2991–3010. https://doi.org/10.1002/1099-1085(200011/12)14:16/17%3C2991::AID-HYP131%3E3.0.CO;2-H

Hynes, H. B. N. (1975). The stream and its valley. SIL Proceedings, 1922-2010, 19(1), 1–15. https://doi.org/10.1080/03680770.1974.11896033

Ilich, A., Lecours, V., Misiuk, B., & Murawski, S. (2025). MultiscaleDTM: Multi-Scale Geomorphometric Terrain Attributes (Version 1.0). Retrieved from https://cran.r-project.org/web/packages/MultiscaleDTM/index.html

Jaeger, K. L., & Olden, J. D. (2012). Electrical Resistance Sensor Arrays as a Means to Quantify Longitudinal Connectivity of Rivers. River Research and Applications, 28(10), 1843–1852. https://doi.org/10.1002/rra.1554

Jensen, C. K., McGuire, K. J., & Prince, P. S. (2017). Headwater stream length dynamics across four physiographic provinces of the Appalachian Highlands. Hydrological Processes, 31(19), 3350–3363. https://doi.org/10.1002/hyp.11259

Jensen, C. K., McGuire, K. J., McLaughlin, D. L., & Scott, D. T. (2019). Quantifying spatiotemporal variation in headwater stream length using flow intermittency sensors. Environmental Monitoring and Assessment, 191(4), 226. https://doi.org/10.1007/s10661-019-7373-8

Jones, C. N., Nelson, N. G., & Smith, L. L. (2019). Featured Collection Introduction: The Emerging Science of Aquatic System Connectivity I. JAWRA Journal of the American Water Resources Association, 55(2), 287–293. https://doi.org/10.1111/1752-1688.12739

Kaplan, N. H., Blume, T., & Weiler, M. (2020). Predicting probabilities of streamflow intermittency across a temperate mesoscale catchment. Hydrology and Earth System Sciences, 24(11), 5453–5472. https://doi.org/10.5194/hess-24-5453-2020

Kindred, T. (2022). Spatial Structure, Temporal Patterns, and Drivers of Stream Drying In the Gibson Jack Watershed, Bannock County, Idaho. Idaho State University, Pocatello, ID.

Kirker, A., Jones, C. N., Peterson, D. M., Tatariw, C., Nettles, J., & Chen, X. (2025). Storage, Connectivity, and Stream Drying in Headwater Systems: Modeling Across Hydrogeomorphic Features. Retrieved from https://www.authorea.com/doi/full/10.22541/essoar.175330904.43292818?commit=4f1b73625bde97ee589993712b5cb42733c86482

Kopaska-Merkel, D. C., Dean, L. S., & Moore, J. D. (2000). HYDROGEOLOGY AND VULNERABILITY TO CONTAMINATION OF MAJOR AQUIFERS IN ALABAMA: AREA 5.

Lee, S., McCarty, G. W., Moglen, G. E., Lang, M. W., Nathan Jones, C., Palmer, M., et al. (2020). Seasonal drivers of geographically isolated wetland hydrology in a low-gradient, Coastal Plain landscape. Journal of Hydrology, 583, 124608. https://doi.org/10.1016/j.jhydrol.2020.124608

Lovill, S. M., Hahm, W. J., & Dietrich, W. E. (2018). Drainage from the Critical Zone: Lithologic Controls on the Persistence and Spatial Extent of Wetted Channels during the Summer Dry Season. Water Resources Research, 54(8), 5702–5726. https://doi.org/10.1029/2017WR021903

Mahoney, D. T., Christensen, J. R., Golden, H. E., Lane, C. R., Evenson, G. R., White, E., et al. (2023). Dynamics of streamflow permanence in a headwater network: Insights from catchment-scale model simulations. Journal of Hydrology, 620, 129422. https://doi.org/10.1016/j.jhydrol.2023.129422

McDonnell, J. J., Sivapalan, M., Vaché, K., Dunn, S., Grant, G., Haggerty, R., et al. (2007). Moving beyond heterogeneity and process complexity: A new vision for watershed hydrology. Water Resources Research, 43(7). https://doi.org/10.1029/2006WR005467

Messager, M. L., Lehner, B., Cockburn, C., Lamouroux, N., Pella, H., Snelder, T., et al. (2021). Global prevalence of non-perennial rivers and streams. Nature, 594(7863), 391–397. https://doi.org/10.1038/s41586-021-03565-5

Miller, D. J., & Dunne, T. (1996). Topographic perturbations of regional stresses and consequent bedrock fracturing. Journal of Geophysical Research: Solid Earth, 101(B11), 25523–25536. https://doi.org/10.1029/96JB02531

Montgomery, D. R., & Dietrich, W. E. (1989). Source areas, drainage density, and channel initiation. Water Resources Research, 25(8), 1907–1918. https://doi.org/10.1029/WR025i008p01907

Montgomery, D. R., & Dietrich, W. E. (1995). Hydrologic Processes in a Low-Gradient Source Area. Water Resources Research, 31(1), 1–10. https://doi.org/10.1029/94WR02270

Moon, S., Perron, J. T., Martel, S. J., Holbrook, W. S., & St. Clair, J. (2017). A model of three-dimensional topographic stresses with implications for bedrock fractures, surface processes, and landscape evolution. Journal of Geophysical Research: Earth Surface, 122(4), 823–846. https://doi.org/10.1002/2016JF004155

Newcomb, S. K., & Godsey, S. E. (2023). Nonlinear Riparian Interactions Drive Changes in Headwater Streamflow. Water Resources Research, 59(10), e2023WR034870. https://doi.org/10.1029/2023WR034870

NOAA National Centers for Environmental Information. (2025). Climate at a Glance: County Time Series [Data set]. Retrieved from https://www.ncei.noaa.gov/access/monitoring/climate-at-a-glance/county/time-series

Peterson, D., N. Jones (2025a). Paint Rock Environmental Data (AIMS_SE_PRF_ENVI), HydroShare, http://www.hydroshare.org/resource/656211b1a1484433a3bc524fb968b4bd

Peterson, D., N. Jones (2025b). Shambley Creek Environmental Data (AIMS_SE_WHR_ENVI), HydroShare, http://www.hydroshare.org/resource/126d2c7b1c8d4889a8ccc454d387b0d8

Peterson, D., N. Jones (2025c). Talladega Environmental Data (AIMS_SE_TAL_ENVI), HydroShare, http://www.hydroshare.org/resource/81c003a7b8474d63a31641a4f375fd18

Peterson, D., N. Jones (2025d). Paint Rock Meteorological Data (AIMS_SE_PRF_approach1_METS), HydroShare, http://www.hydroshare.org/resource/4089918c0a494bfeb19be0421a33d297

Peterson, D., N. Jones (2025e). Shambley Creek Meteorological Data (AIMS_SE_WHR_approach1_METS), HydroShare, http://www.hydroshare.org/resource/33823d8603ce439fbba48fbcbba22da4

Peterson, D., N. Jones (2025f). Talladega Meteorological Data (AIMS_SE_TAL_approach1_METS), HydroShare, http://www.hydroshare.org/resource/281cd7627629481dbdc7d4ccf6fcfbcc

Peterson, D., N. Jones (2025g). Paint Rock Stream Temperature, Intermittency, and Conductivity Data (AIMS_SE_PRF_approach1_STIC), HydroShare, http://www.hydroshare.org/resource/d57338ebfb0240f58e8de37ddacf9426

Peterson, D., N. Jones (2025h). Shambley Creek Stream Temperature, Intermittency, and Conductivity Data (AIMS_SE_WHR_approach1_STIC), HydroShare, http://www.hydroshare.org/resource/dc623510ed1847f8abe1275904472c44

Peterson, D., N. Jones (2025i). Talladega Stream Temperature, Intermittency, and Conductivity Data (AIMS_SE_TAL_approach1_STIC), HydroShare, http://www.hydroshare.org/resource/ff306bec9fb24e52aa809dbb4d074731

Peterson, D. M., Jones, C. N., Plattner, A. M., Shogren, A. J., & Godsey, S. E. (2025). Using Hydrogeomorphic Features to Quantify Structural and Functional Hydrologic Connectivity in a Coastal Plain Headwater Stream. Water Resources Research, 61(8), e2024WR038533. https://doi.org/10.1029/2024WR038533

Plont, S., Peterson, D. M., Smith, C. R., Bond, C. T., Tchamba, A. L. K., Wolford, M. A., et al. (2026). Hydrologic, biogeochemical, microbial, and macroinvertebrate responses to network expansion, contraction, and disconnection across headwater stream networks with distinct physiography in Alabama, USA. Earth System Science Data, 4885–4914. https://doi.org/10.5194/essd-18-4885-2026

Plont, S., S. Speir, D. Peterson, N. Jones (2025a). AIMS Paint Rock Continuous Discharge at Watershed Outlet Data (AIMS_SE_PRF_DISC), HydroShare, http://www.hydroshare.org/resource/043fc07f0c3b47bcabbd0bf5600d929f

Plont, S., S. Speir, D. Peterson, N. Jones (2025b). AIMS Shambley Creek Continuous Discharge at Watershed Outlet Data (AIMS_SE_WHR_DISC), HydroShare, http://www.hydroshare.org/resource/535797126b134ceaab9838df0ca00885

Plont, S., M. Wolford, K. Zarek, D. Peterson, N. Jones, S. Speir (2025). AIMS Talladega Continuous Discharge at Watershed Outlet Data (AIMS_SE_TAL_DISC), HydroShare, http://www.hydroshare.org/resource/fc7ae2d28e3c481d805902a79af90a95

Ponta, G. (2018). Geologic Framework of Karst Aquifer Systems in Alabama. Sinkhole Conference 2018. Retrieved from https://digitalcommons.usf.edu/sinkhole_2018/ProceedingswithProgram/Appalachian_Karst/6

Prancevic, J. P., & Kirchner, J. W. (2019). Topographic Controls on the Extension and Retraction of Flowing Streams. Geophysical Research Letters, 46(4), 2084–2092. https://doi.org/10.1029/2018GL081799

Prancevic, J. P., Seybold, H., & Kirchner, J. W. (2025). Variability of flowing stream network length across the US. Science, 387(6735), 782–786. https://doi.org/10.1126/science.ado2860

Pringle, C. M. (2001). Hydrologic Connectivity and the Management of Biological Reserves: A Global Perspective. Ecological Applications, 11(4), 981–998. https://doi.org/10.1890/1051-0761(2001)011[0981:HCATMO]2.0.CO;2

R Core Team. (2024). R: A Language and Environment for Statistical Computing. Vienna, Austria: R Foundation for Statistical Computing. Retrieved from https://www.R-project.org/

Rinderer, M., van Meerveld, H. J., & Seibert, J. (2014). Topographic controls on shallow groundwater levels in a steep, prealpine catchment: When are the TWI assumptions valid? Water Resources Research, 50(7), 6067–6080. https://doi.org/10.1002/2013WR015009

Rinderer, M., Ali, G., & Larsen, L. G. (2018). Assessing structural, functional and effective hydrologic connectivity with brain neuroscience methods: State-of-the-art and research directions. Earth-Science Reviews, 178, 29–47. https://doi.org/10.1016/j.earscirev.2018.01.009

Rutter, A. J., Morton, A. J., & Robins, P. C. (1975). A Predictive Model of Rainfall Interception in Forests. II. Generalization of the Model and Comparison with Observations in Some Coniferous and Hardwood Stands. Journal of Applied Ecology, 12(1), 367–380. https://doi.org/10.2307/2401739

Senatore, A., Micieli, M., Liotti, A., Durighetto, N., Mendicino, G., & Botter, G. (2021). Monitoring and Modeling Drainage Network Contraction and Dry Down in Mediterranean Headwater Catchments. Water Resources Research, 57(6), e2020WR028741. https://doi.org/10.1029/2020WR028741

Soil Survey Staff, Natural Resources Conservation Service, USDA. Accessed March 2025. Web Soil Survey [Data set]. Retrieved from https://websoilsurvey.nrcs.usda.gov/app/

Swenson, G. A. (1954). Soil Survey of Jackson County, Alabama. U.S. Department of Agriculture, Soil Conservation Service.

Swank, W., DeBano, L., & Nelson, D. (1989). Effects of Timber Management Practices on Soil and Water. In The Scientific Basis for Silvicultural and Management Decisions in the National Forest System. U.S. Department of Agriculture, Forest Service.

U.S. Geological Survey (USGS), 2024, Annual NLCD Collection 1 Science Products: U.S. Geological Survey data release, https://doi.org/10.5066/P94UXNTS

van Meerveld, H. J. I., Kirchner, J. W., Vis, M. J. P., Assendelft, R. S., & Seibert, J. (2019). Expansion and contraction of the flowing stream network alter hillslope flowpath lengths and the shape of the travel time distribution. Hydrology and Earth System Sciences, 23(11), 4825–4834. https://doi.org/10.5194/hess-23-4825-2019

Ward, A. S., Schmadel, N. M., & Wondzell, S. M. (2018). Simulation of dynamic expansion, contraction, and connectivity in a mountain stream network. Advances in Water Resources, 114, 64–82. https://doi.org/10.1016/j.advwatres.2018.01.018

Ward, J. V. (1989). The Four-Dimensional Nature of Lotic Ecosystems. Journal of the North American Benthological Society, 8(1), 2–8. https://doi.org/10.2307/1467397

Warix, S. R., Navarre-Sitchler, A., Manning, A. H., & Singha, K. (2023). Local Topography and Streambed Hydraulic Conductivity Influence Riparian Groundwater Age and Groundwater-Surface Water Connection. Water Resources Research, 59(9), e2023WR035044. https://doi.org/10.1029/2023WR035044

Warix, S. R., Godsey, S. E., Lohse, K. A., & Hale, R. L. (2021). Influence of groundwater and topography on stream drying in semi-arid headwater streams. Hydrological Processes, 35(5), e14185. https://doi.org/10.1002/hyp.14185

Whiting, J. A., & Godsey, S. E. (2016). Discontinuous headwater stream networks with stable flowheads, Salmon River basin, Idaho. Hydrological Processes, 30(13), 2305–2316. https://doi.org/10.1002/hyp.10790

Wu, Q., & Brown, A. (2022). whitebox: “WhiteboxTools” R Frontend. R package version 2.2.0. Retrieved from https://CRAN.R-project.org/package=whitebox

Young-Robertson, J. M., Bolton, W. R., Bhatt, U. S., Cristóbal, J., & Thoman, R. (2016). Deciduous trees are a large and overlooked sink for snowmelt water in the boreal forest. Scientific Reports, 6(1), 29504. https://doi.org/10.1038/srep29504

Zanetti, F., Durighetto, N., Vingiani, F., & Botter, G. (2022). Technical note: Analyzing river network dynamics and the active length–discharge relationship using water presence sensors. Hydrology and Earth System Sciences, 26(13), 3497–3516. https://doi.org/10.5194/hess-26-3497-2022

Zarek, K., Jones, C. N., Peterson, D. M., Plont, S., Shogren, A. J., Tatariw, C., et al. (2025). Investigating Spatial and Temporal Nitrogen Dynamics in a Forested Headwater Stream Over the Course of an Annual Drying Event. Journal of Geophysical Research: Biogeosciences, 130(4), e2024JG008522. https://doi.org/10.1029/2024JG008522

Zimmer, M. A., & McGlynn, B. L. (2017). Bidirectional stream–groundwater flow in response to ephemeral and intermittent streamflow and groundwater seasonality. Hydrological Processes, 31(22), 3871–3880. https://doi.org/10.1002/hyp.11301

Zimmer, M. A., & McGlynn, B. L. (2018). Lateral, Vertical, and Longitudinal Source Area Connectivity Drive Runoff and Carbon Export Across Watershed Scales. Water Resources Research, 54(3), 1576–1598. https://doi.org/10.1002/2017WR021718

Zimmer, M. A., Burgin, A. J., Kaiser, K., & Hosen, J. (2022). The unknown biogeochemical impacts of drying rivers and streams. Nature Communications, 13(1), 7213. https://doi.org/10.1038/s41467-022-34903-4

Zipper, S., Wheeler, C. T., Peterson, D. M., Cook, S. C., Godsey, S. E., & Aho, K. (2025). STICr: An open-source package and workflow for stream temperature, intermittency, and conductivity (STIC) data. Environmental Modelling & Software, 190, 106484. https://doi.org/10.1016/j.envsoft.2025.106484

Zipper, S. C., Hammond, J. C., Shanafield, M., Zimmer, M., Datry, T., Jones, C. N., et al. (2021). Pervasive changes in stream intermittency across the United States. Environmental Research Letters, 16(8), 084033. https://doi.org/10.1088/1748-9326/ac14ec

Supporting Information for

Stream Network Dynamics in Three Watersheds in the Southeastern USA Highlight Interactions Between Physiographic Variables

Delaney M. Peterson[1,2], C. Nathan Jones[1], Kaci Zarek[1,3], Michelle Wolford[1], Chelsea R. Smith[1], Charles T. Bond[4], Stephen Plont[1], Maggi Kraft[5], Shannon Speir[6], Sam Zipper[7,8], Sarah E. Godsey[5], Jonathan P. Benstead[1], Arial J. Shogren[1], Kevin A. Kuehn[4], and Carla L. Atkinson[1]

[1]Department of Biological Sciences, University of Alabama, Tuscaloosa, AL, USA; [2]Department of Biological and Ecological Engineering, Oregon State University, Corvallis, OR, USA; [3]Department of Ecology and Evolutionary Biology, Cornell University, Ithaca, NY, USA; [4]School of Biological, Environmental, and Earth Sciences, University of Southern Mississippi, Hattiesburg, MS, USA; [5]Department of Geosciences, Idaho State University, Pocatello, ID, USA; [6]Department of Crop, Soil, and Environmental Sciences, University of Arkansas, Fayetteville, AR, USA; [7]Kansas Geological Survey, University of Kansas, Lawrence, KS, USA; [8]Department of Geology, University of Kansas, Lawrence, KS, USA.

Contents of this file

Text S1 to S2

Figures S1 to S12

Tables S1 to S3

Introduction

This document contains more detailed site information (Text S1) and data collection (Text S2), study design and sensor placement (Figures S4-7), and description of all physiographic metrics (Table S1) to provide further details on methodology. Additionally, this document contains additional sensitivity analyses (Table S2, Figures S8-10), statistical results (Table S3), as well as additional figures that provide more context to results (Figure S1-3, 11-12).

Text S1 – Detailed Site Descriptions.

We instrumented three research watersheds across a physiographic gradient in Alabama, USA to evaluate network expansion and contraction across comparably-sized non-perennial streams. In addition to the details provided in Section 2.1 and Table 1, we have included more detailed watershed characteristics below.

Appalachian Plateaus Research Watershed

The research watershed in the Appalachian Plateau province drains 2.97km^2 of Fanning Hollow and Miller Mountain to form the steep headwaters of Burks Creek, within the larger Paint Rock River and Tennessee River basins. Physiographically, this research watershed is in the Jackson Mountains district, defined by flat sandstone-capped ridges that are highly dissected by dendritic stream networks that form V-shaped ravines and rock-walled gorges as they grade into wider valley bottoms (Swenson, 1945; Sapp & Emplaincourt, 1975).

Geologically, this watershed cuts through and exposes several distinct sedimentary lithologic units. In this region, the plateaus are primarily from the Pottsville and Pennington Formations, which are underlain by the Bangor limestone, Monteagle limestone, and Tuscumbia limestone units, respectively (Szabo et al., 1988; Ponta, 2018). The Pottsville and Pennington formations are primarily sandstones and shales interbedded with limestone, dolomite, and mudstones, whereas the three underlying units are primarily limestone and dolomite with some chert concretions in the Tuscumbia unit (Szabo et al., 1988). Further, the Bangor, Monteagle, and Tuscumbia limestone units are all karst, with the majority of caves in the state occurring in the Bangor limestone unit (Ponta, 2018). The Pottsville formation, Bangor limestone, and Tuscumbia limestone are the primary water-bearing units for the region, with the Pottsville formation being the largest water source in the region and the Bangor limestone being an unconfined karst aquifer that discharges through many springs (Ponta, 2018). This watershed primarily has SSURGO soil map units of Limestone rockland rough and Muskingum Rough stony land. These map units consist of highly organic soils and limestone residuum in the headwaters, and more developed, argillic soils in the valley bottom (Soil Survey Staff, 2025). The dominant soil series are the Barfield, Gorgas, and Egam series.

This watershed is located in the Plateau Escarpment level IV ecoregion, and therefore the forest structure is primarily deciduous, with mixed oak species (chestnut oak, white and red oaks) in the upper slopes, mesic forest (beech, yellow-poplar, sugar maple, basswood, ash, buckeye) in the middle and lower slopes, and some hemlock and river birch in the riparian zones and floodplain terraces near the outlet (Griffith et al., 2001).

Piedmont Research Watershed

The research watershed in the Piedmont province drains 0.92km^2 of Rattlesnake Mountain to form the headwaters of Pendergrass Creek, within the larger Coosa River and Mobile-Tombigbee River basins. Physiographically, this watershed is in the Northern Piedmont

Upland district, defined as a well-dissected mature upland in the transition between the nearby Ridge and Valley and Coastal Plain regions (Kopaska-Merkel et al., 2000).

Geologically, this watershed is underlain by fractured metamorphic lithologic units. The watershed is located in the Talladega belt near the Talladega fault, and lies within the exposed Lay Dam formation, which is made up of interbedded phyllite, metasiltstone, and quartzite members (Szabo et al, 1988; Cook, 1982; Kopaska-Merkel et al., 2000). Productivity of the groundwater system in the Piedmont is driven by fractures rather than geologic material (Kopaska-Merkel et al., 2000), and the proximity of this location to the Talladega fault has likely resulted in a productive groundwater system where the fractures intersect with the soil and ground surface. This watershed has highly weathered soils, with the primary soil series being the Cheaha, Tatum, and Fruithurst, as well as some more organic, fine-grained soils near the watershed outlet (Soil Survey Staff, 2025; Zarek et al., 2025).

The watershed is located within the Talladega Upland level IV ecoregion, and therefore has a mixed deciduous-coniferous forest structure. The region has an oak-hickory-pine natural vegetation type and historically contained unique montane longleaf pine communities (Griffith et al., 2001). The watershed now contains primarily pine and oak species (loblolly, longleaf, mixed red and white oaks; Feminella, 1996; Zarek et al., 2025). While the larger region has a long-term land-use history of intensive cultivation (Trimble, 2008, Griffith et al., 2001), the region transitioned to silviculture around the turn of the 20th century. Additionally, the US Forest Service maintains a regular burn schedule within the National Forest to preserve the longleaf pine and endangered red cockaded woodpecker habitat. As a result, this watershed experienced low-intensity prescribed burns in the early spring of both 2022 and 2024.

Coastal Plain Research Watershed

The research watershed in the Coastal Plain province drains 0.70km^2 of the headwaters of Shambley Creek, within the larger Sipsey River and Mobile-Tombigbee River basins. Physiographically, this watershed is in the Fall Line Hills district, defined by low-gradient sandy uplands that are dissected by severely entrenched streams (Kidd & Lambeth, 1995; Fenneman, 1938).

Geologically, this watershed is underlain by sedimentary lithologic units. The watershed is located in the exposed Eutaw Formation, which consists of interbedded sand and clay layers (Szabo et al., 1988). This formation includes the Tombigbee Sand Member, and the shallow depth to this aquifer results in this unit being an integral water-bearing unit for the region (Wahl, 1966). The primary soils present in this watershed are the Magnolia, Shubuta, Falaya, and Ochlockonee series (Soil Survey Staff, 2025).

Greene County, as well as the larger Coastal Plain of the Southeastern US, has a long-term land-use legacy of intensive agriculture that has resulted in soil degradation and erosion (Trimble, 2008; AL Historical Commission, 2002). The region was heavily used for cotton farming throughout the 19th century before conversion to pine plantations and other silvicultural practices during the southern USA lumber boom circa 1900 (AL Historical Commission, 2002; Fickle, 2014). This property was purchased by the Weyerhaeuser Company and has been used for both rotational pine harvest and forest biofuel research from 2010-2016 (Chescheir et al., 2018; Dobbs, 2016). The watershed is located within the larger Fall Line Hills level IV ecoregion, and therefore has a historic forest structure of mixed coniferous and deciduous species (primarily oaks, hickory, and pines, with some longleaf reintroduction efforts; Griffith et al., 2001).

Text S2 – Densiometer Measurements.

We derived relative proportions of riparian vegetation types from densiometer measurements taken throughout the watershed across seasons. In short, densiometer measurements of canopy coverage were taken at seven consistent locations within each watershed at least four times throughout the two-year study period (see "LTM" site locations in Figure S4). To ensure precision, these measurements were taken in the channel adjacent to permanent project infrastructure (i.e., stilling wells). Additional densiometer measurements were taken at all 49 sensor locations in the Piedmont research watershed once in June 2022. Each individual measurement consisted of averaging four to six canopy cover measurements within a stream reach, and canopy cover was calculated as the total number of covered quadrants within the densiometer divided by the total number of quadrants.

Using both temporally and spatially distributed densiometer measurements, relative proportions of vegetation types were calculated by comparing late-winter leaf-off measurements (i.e., a proxy for coniferous vegetation) to late-summer leaf-on measurements. For each location, the leaf-off measurements were subtracted from their respective leaf-on measurements to calculate relative proportion of deciduous vegetation. These calculations were then aggregated by HGF, and the percent of deciduous vegetation was calculated as the average ratio of deciduous vegetation to the total leaf-on measurement x 100. The percent of coniferous vegetation for each HGF was calculated as the average ratio of leaf-off measurement to leaf-on measurement x 100. These data were included in the multidimensional analysis of the HGFs (see Figures S13-15), but all other vegetation analyses used 2024 NLCD data as described in Section 2.3.

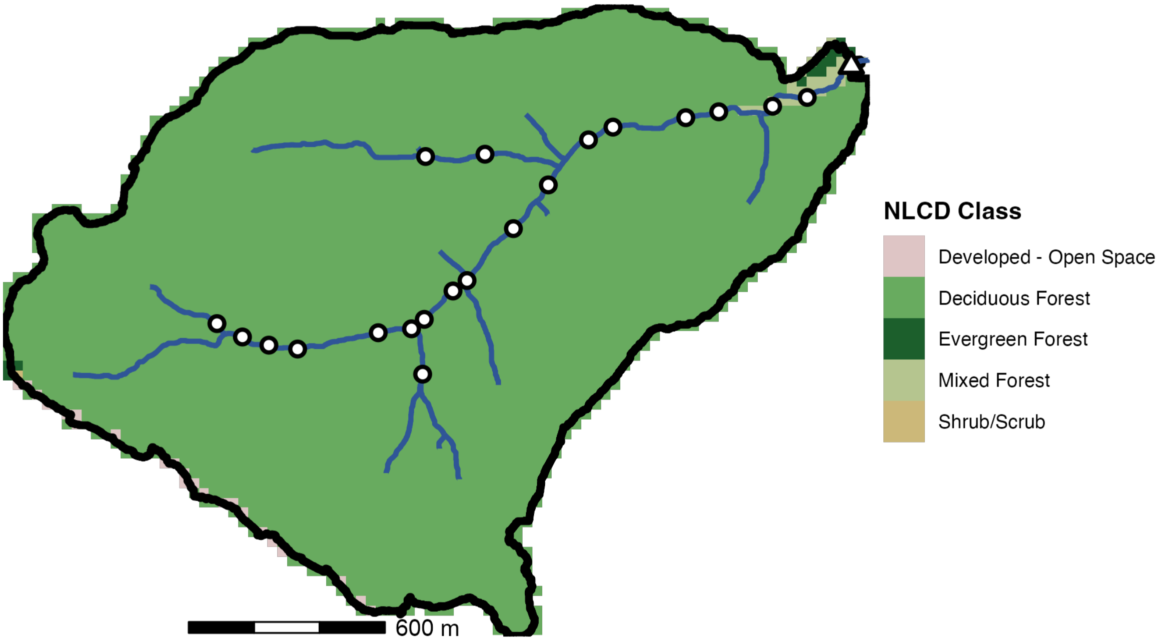

Figure S1. National Land Cover Database (NLCD) classes for the Appalachian Plateaus watershed. The stream network in indicated in blue, with STIC sensors along the stream as white circles. The outlet monitoring location is indicated by the white triangle.

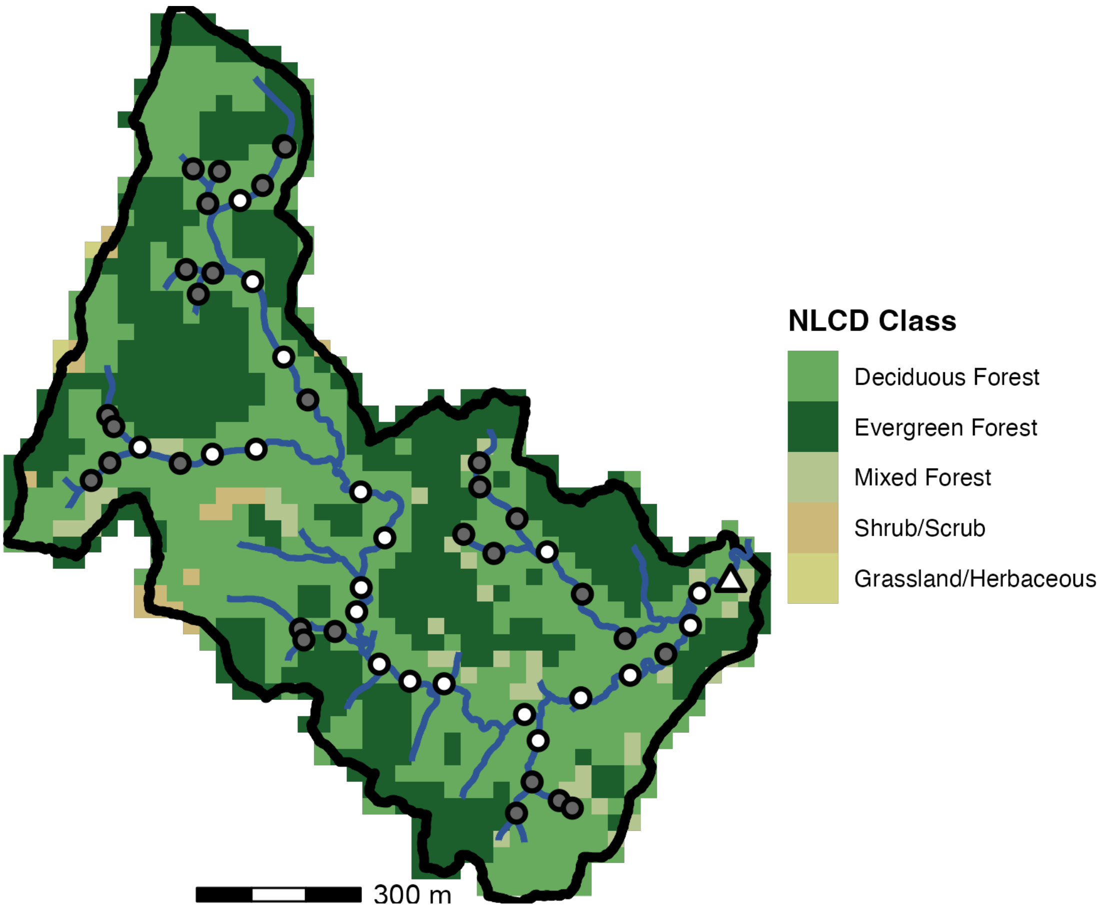

Figure S2. National Land Cover Database (NLCD) classes for the Piedmont watershed. The stream network is indicated in blue, with all STIC sensors (circles) colored as permanent (white) or high-density (grey). The watershed outlet sampling location is indicated by the white triangle.

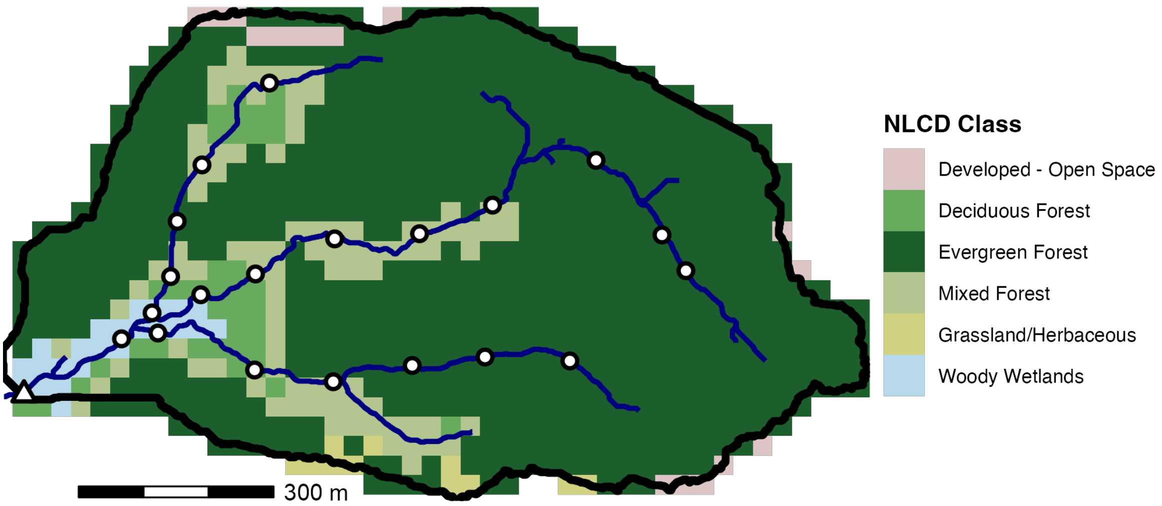

Figure S3. National Land Cover Database (NLCD) classes for the Coastal Plain watershed. The stream network in indicated in blue, with STIC sensors along the stream as white circles. The outlet monitoring location is indicated by the white triangle.

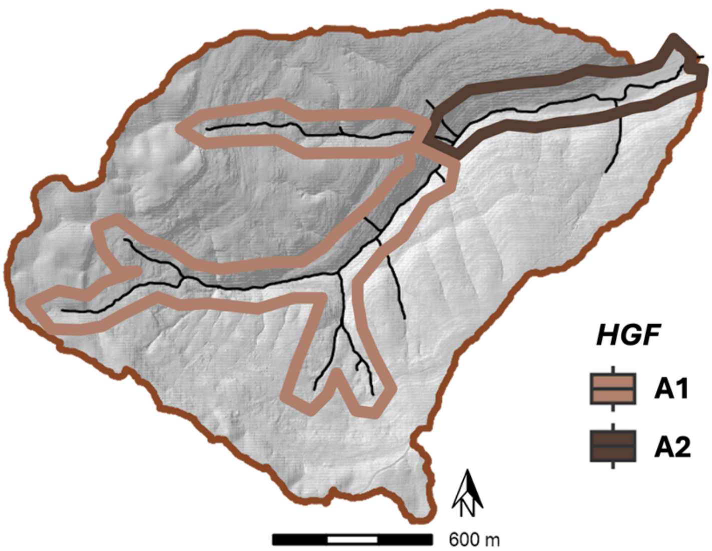

Figure S4. Hydrogeomorphic features of the instrumented portions of the Appalachian Plateaus watershed.

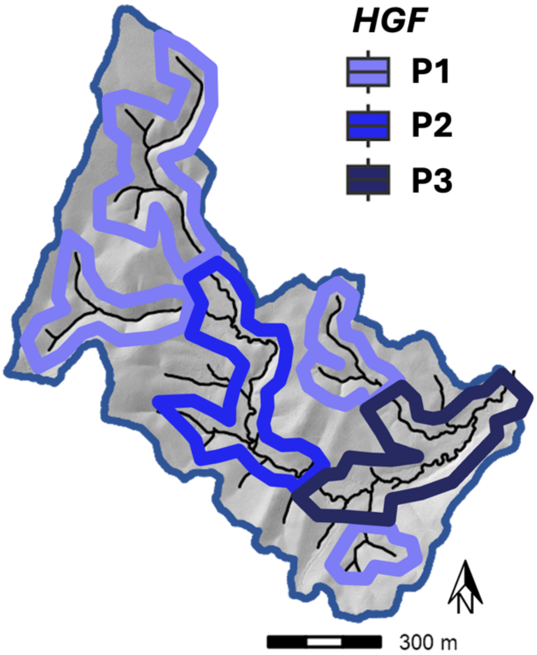

1342

1343 **Figure S5.** Hydrogeomorphic features of the instrumented portions of the Piedmont
1344 watershed.

1345

1346

1347

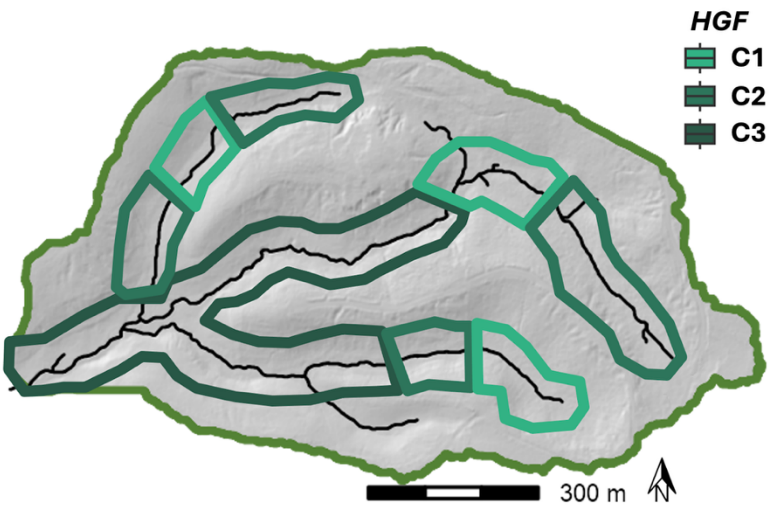

1348

1349 **Figure S6.** Hydrogeomorphic features of the instrumented portions of the Coastal Plain
1350 watershed.

1351

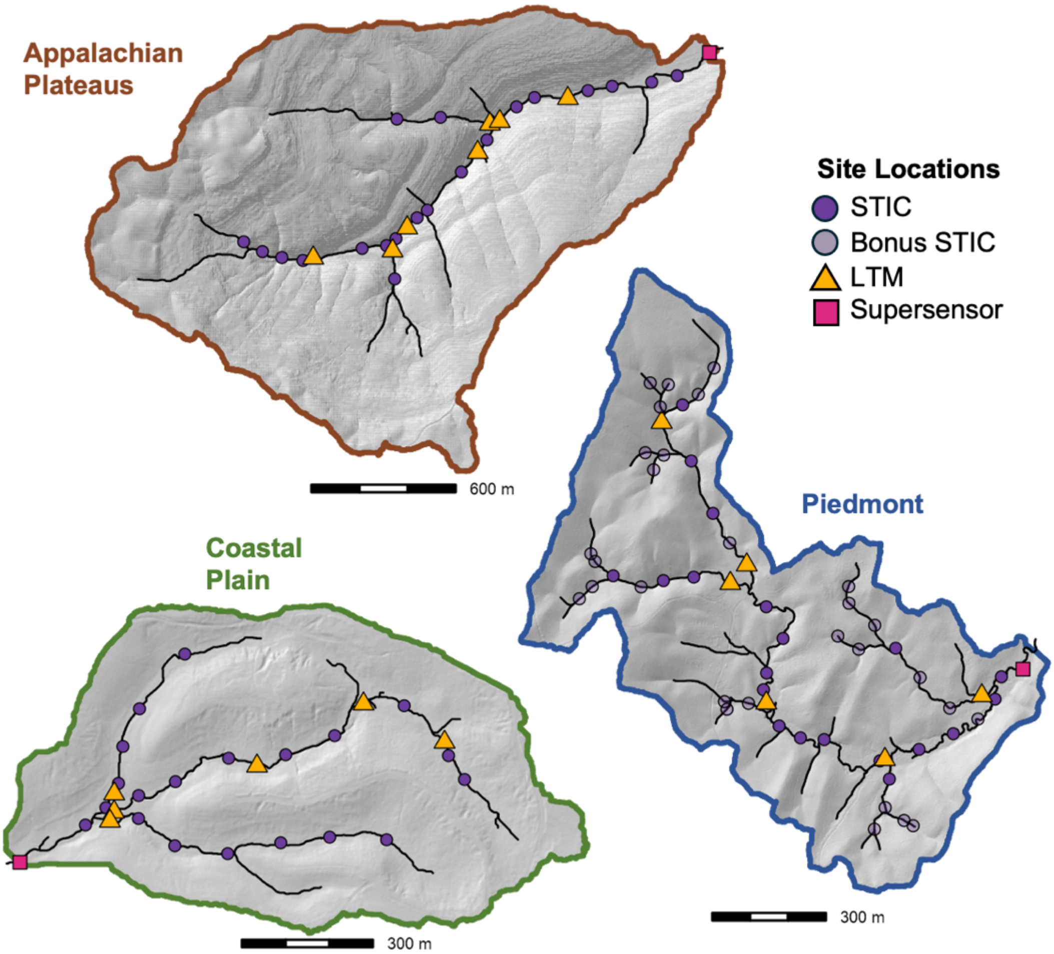

Figure S7. Sensor networks of the three research watersheds. Each watershed shows the three different types of sensors present (STIC = water presence/absence; Bonus STIC = the high-density additional sensors deployed in the Piedmont research watershed; LTM = Long-Term Monitoring locations, where stilling wells and piezometers were deployed in the channel and regular water sampling occurred; Supersensor = the outlet monitoring location, where water level and discharge were measured, as well as a high-frequency water quality sonde).

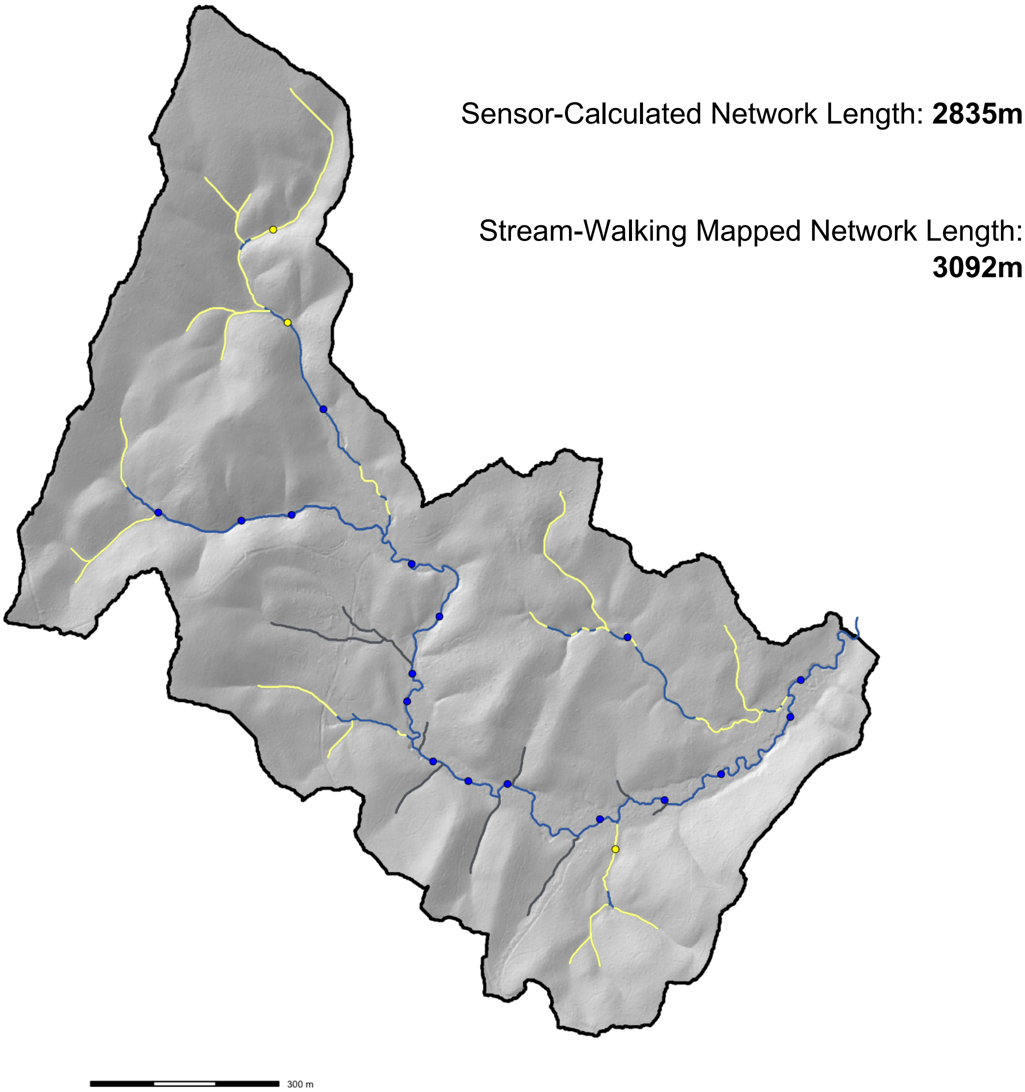

Figure S8. Sensor network results compared to network mapping on 26 August, 2023. Sensor observations are indicated by colored points, where blue indicates a “wet” daily value and yellow indicates “dry”. The stream network is colored by stream-walking network length observations, where reaches observed wet are indicated by blue lines and reaches observed dry in yellow. Respective total lengths are noted on the top right.

Table S1. A description of all physiographic metrics calculated for this study.

Category	Metric	Scale	Description	Reference
Topographic	Slope	Site (1m)	Slope (%) extracted from the DEM at the sensor location using *wbt_slope()*	Lindsay, 2016; Florinsky, 2016
	Buffer slope	Site (5m)	Slope (%) averaged in a 5m circular buffer around the sensor location using *wbt_slope()*	sensu Warix et al., 2023; Lindsay, 2016
	Channel Slope	Reach (25m)	Slope (%) of only the channel network averaged across a 25m reach using *wbt_stream_slope_continuous()*	Lindsay, 2016
	Curvature	Site (1m)	Mean curvature (m^{-1}) of the topographic surface using *wbt_mean_curvature()*, doubled with the sign reversed to following Prancevic & Kirchner (2019)	Wilson, 2018; Lindsay, 2016; Prancevic & Kirchner (2019)
	Distance to outlet	Site	In-stream distance (m) from watershed outlet to sensor location using *wbt_distance_to_outlet()*	Lindsay, 2016
	Drainage area	Site	Contributing area (m^2) draining to an individual sensor location using *wbt_d8_flow_accumulation()*	Lindsay, 2016
	Topographic Wetness Index (TWI)	Site (1m)	TWI of the sensor location calculated as **ln(catchment area / tan(slope))** using *wbt_wetness_index()*	Beven & Kirkby, 1979; Lindsay, 2016
	Topographic Position Index (TPI)	Site (5m)	TPI of the 5m circular buffer around the sensor calculated as (focal elevation - mean(all other cell elevations)) using *TPI()*	Ilich et al., 2025
	Drainage density	Site	Upstream length (m) divided by drainage area of the sensor location	Montgomery & Dietrich, 1989; Godsey & Kirchner, 2014
	β, network expansion exponent	Network	The exponent of the relationship between stream length and discharge at the outlet, calculated as ($L \propto Q_o^{\beta}$)	Godsey & Kirchner, 2014; Prancevic & Kirchner, 2019
Soil	Saturated hydraulic conductivity	HGF	Ability of saturated pores to transmit water (μm/s) in the upper 100 cm of the soil profile for each soil map unit, derived from soil structure, porosity, and texture data	Soil Survey Staff, 2025

	Percent sand	HGF	Sand textural content (%) in the total soil profile as a weighted average for each soil map unit	Soil Survey Staff, 2025
	Percent silt	HGF	Silt textural content (%) in the total soil profile as a weighted average for each soil map unit	Soil Survey Staff, 2025
	Percent clay	HGF	Clay textural content (%) in the total soil profile as a weighted average for each soil map unit	Soil Survey Staff, 2025
	Organic matter content	HGF	Organic matter (%) by weight in the upper 50 cm of the soil profile for each soil map unit	Soil Survey Staff, 2025
Geology	Primary lithologic unit	HGF	Most surficial geologic layer; identified as parent material from soil surveys for each soil map unit	Soil Survey Staff, 2025; Szabo et al., 1988
	Depth to bedrock	HGF	Average depth (cm) to a lithologic restrictive layer for each soil map unit	Soil Survey Staff, 2025
Vegetation	Percent coniferous vegetation	Site	Relative percentage of the site-specific subwatershed area with an "evergreen forest" NLCD classification	
	Percent deciduous vegetation	HGF	Relative percentage of riparian deciduous vegetation (%), derived from the difference between leaf off and leaf on in-stream densiometer measurements (Text S2)	

Table S2. Sensitivity analysis for the relationship between temporal resolution and expansion exponent, β.

Watershed	15-minute β	Mean Daily β	Daily Noon β
Coastal Plain	0.085 ± 0.076	0.121 ± 0.098	**0.127** ± 0.087
Appalachian Plateaus	0.204 ± 0.085	0.161 ± 0.092	**0.185** ± 0.086
Piedmont (n = 20)	0.059 ± 0.033	0.082 ± 0.039	**0.076** ± 0.039
Piedmont (n = 49)	0.058 ± 0.048	0.061 ± 0.047	**0.059** ± 0.048

Note: β in bold were used in analyses.

Table S3 HGF-scale statistical results

Variable of Interest	Appalachian Plateaus p-value	Piedmont p-value	Coastal Plain p-value
Percent Wet	0.14	**0.05**	**0.03**
Saturated hydraulic conductivity	**0.03**	**0.0003**	0.47
Percent sand	**0.03**	**0.01**	0.44
Percent silt	**0.03**	**0.01**	0.69
Percent clay	**0.03**	**0.01**	0.52
Organic matter content	**0.03**	**0.0003**	0.69
Depth to bedrock	**0.03**	**0.0003**	n/a[a]

Percent deciduous vegetation	0.70	0.56	0.85
Percent coniferous vegetation	0.14	**0.01**	0.17

[a]not applicable as there was no measurable depth to bedrock in the Coastal Plain

Note. Variables in bold are statistically significant ($p < 0.05$)

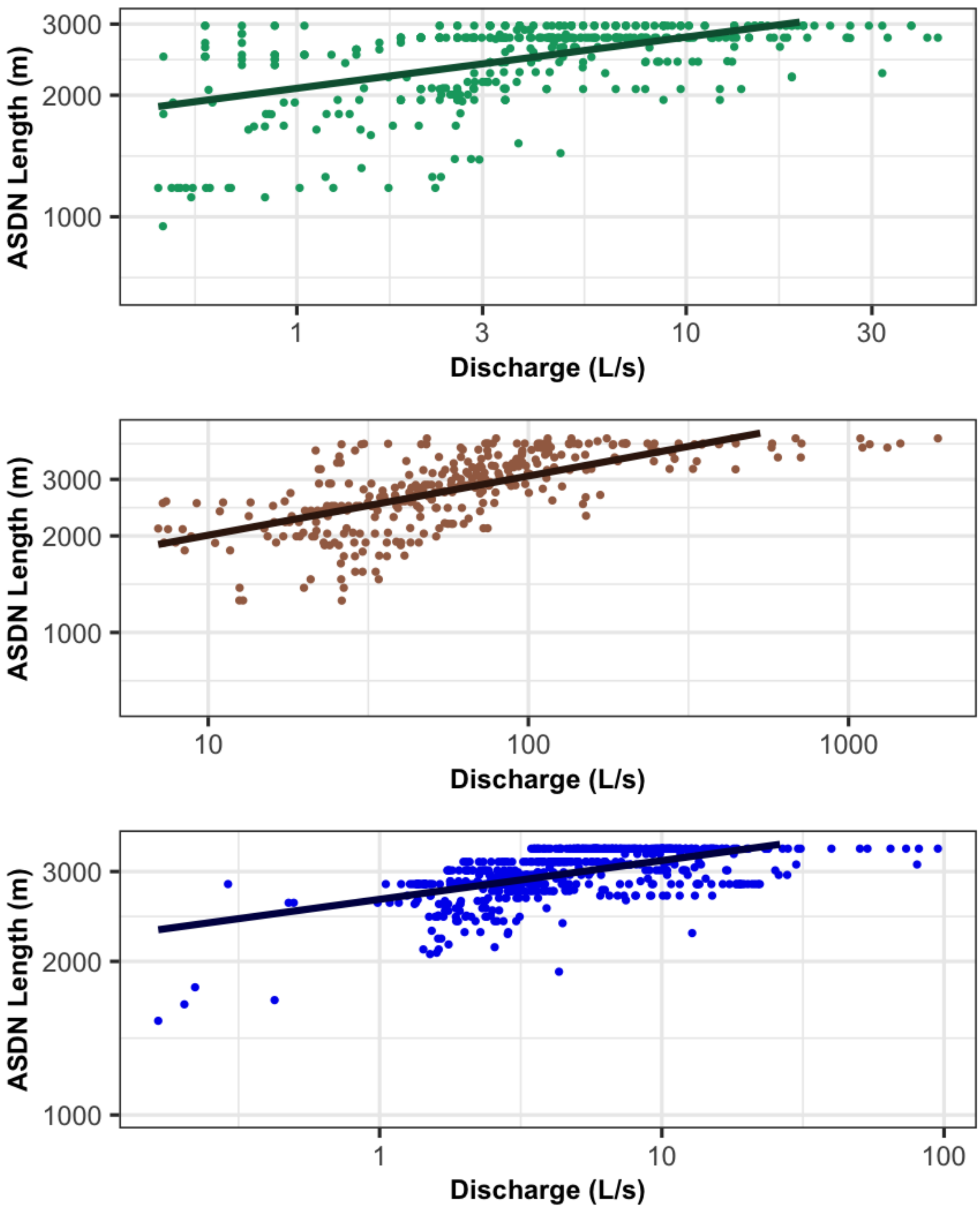

Figure S9. Daily observations of outlet discharge (Q) and network length used to calculate observed expansion exponents (β) for each watershed. Coastal Plain is indicated in green, Appalachian Plateaus in brown, and Piedmont in blue.

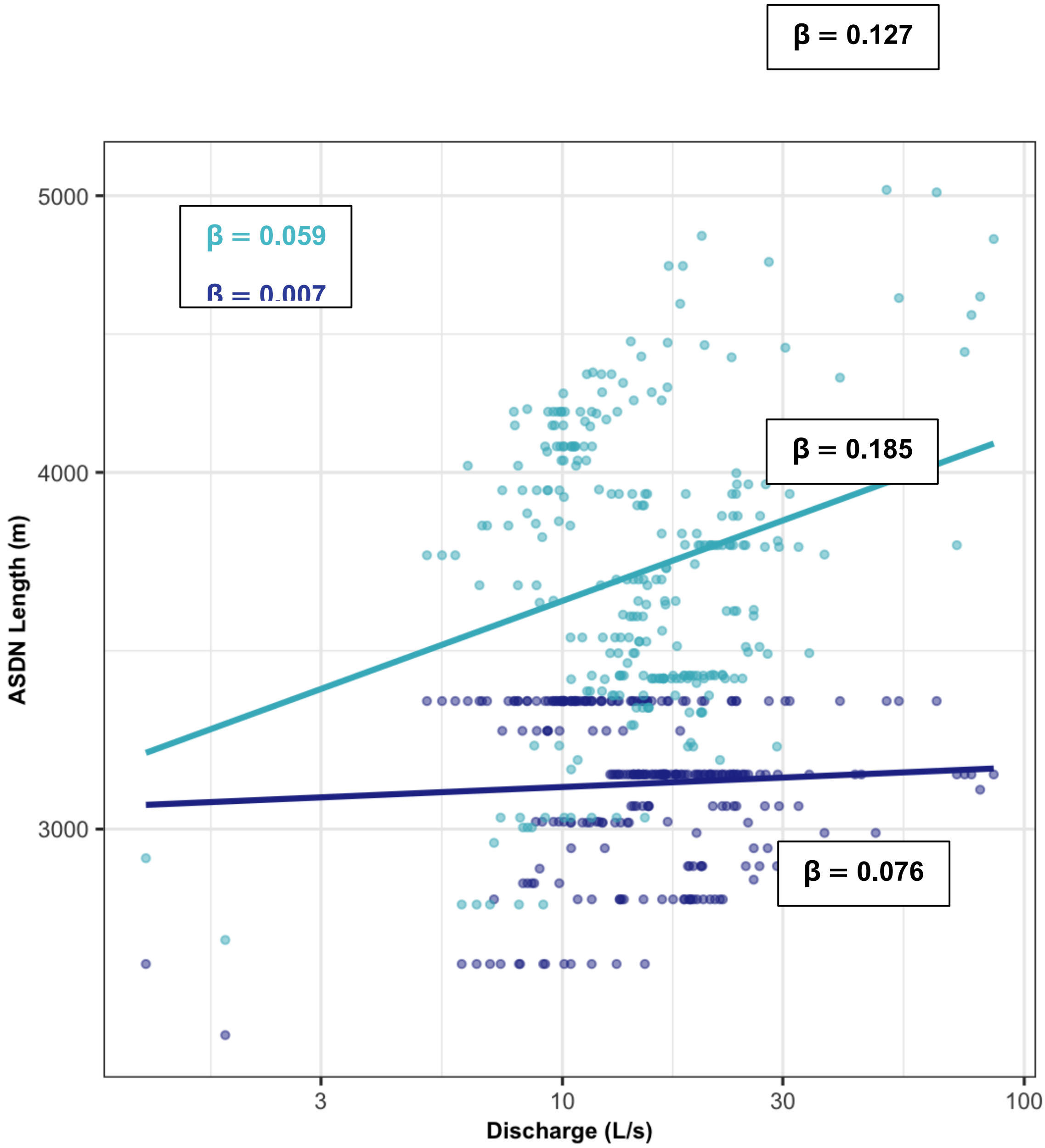

Figure S10. Daily observations of outlet discharge (Q) and network length used to calculate observed expansion exponents (β) for both the high density (n = 49; light blue) and permanent (n = 20; dark blue) sensor networks in the Piedmont watershed. Note: data from the 11-month period of high-density deployment is used here to ensure comparability, rather than the two water years used in other analyses.

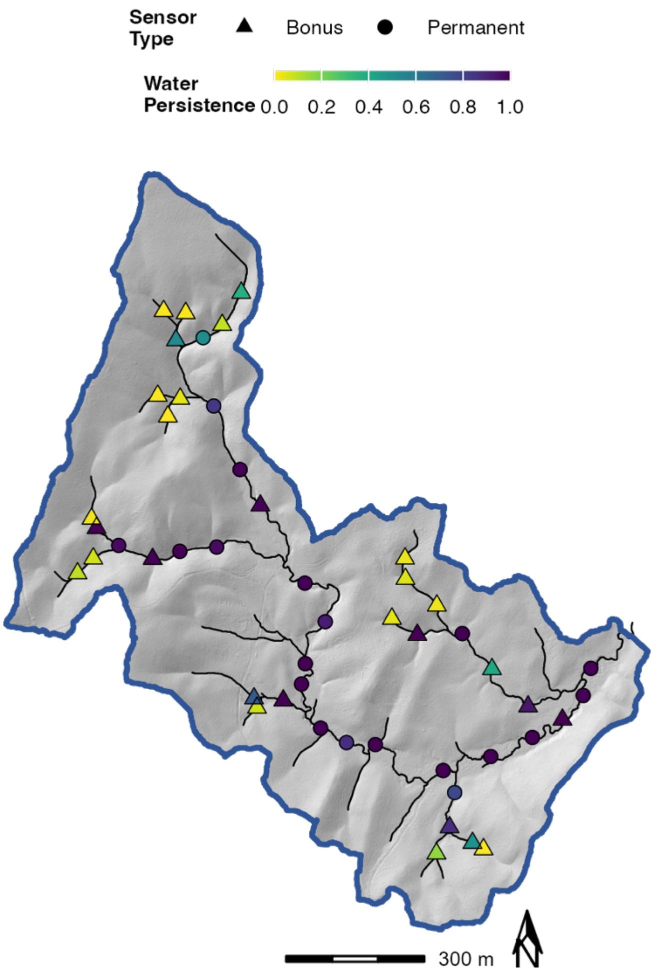

Figure S11. The Piedmont research watershed, with each site colored by water persistence over the 11-month period of high-density sensor deployment. Permanent sensors (n = 20) are indicated by circles, and the additional high-density network sensors (n = 29) are indicated by triangles. Water persistence is measured as the proportion of days the sensor recorded "wet" from May 2022 through April 2023.

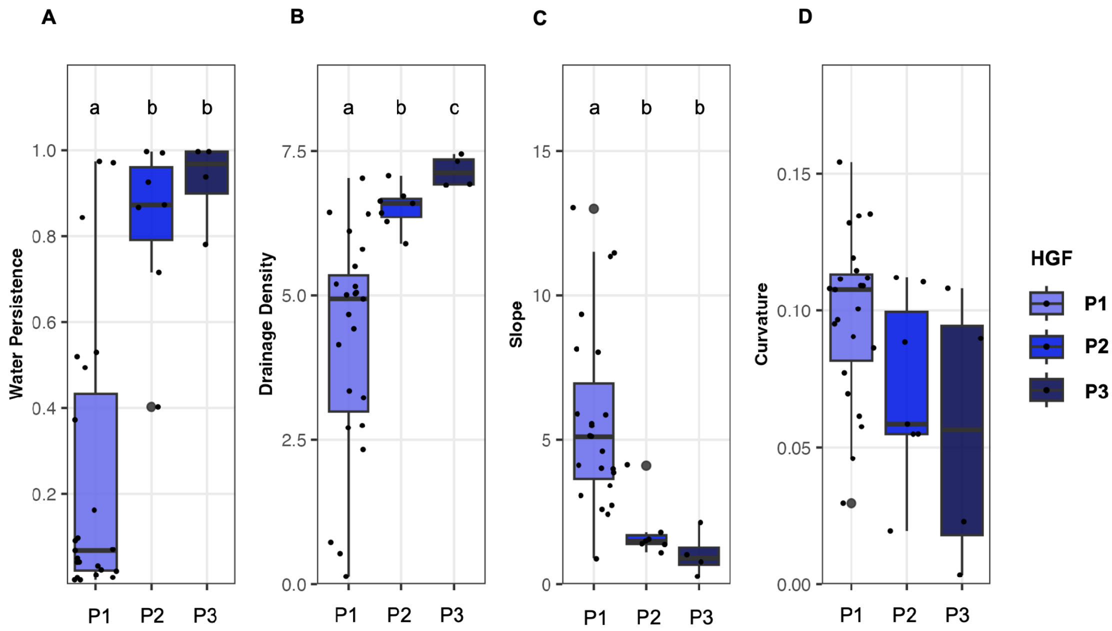

Figure S12. Boxplots for water persistence (A) and the three primary topographic metrics (B-D) for all sensors in the Piedmont high-density network (n = 49). Sensors are grouped by hydrogeomorphic feature (HGF, see legend and x axis). Significance between groups is denoted by letters above each group ($p < 0.05$). See Figure 8 for continuous relationships between water persistence (A) and subsequent topographic metrics (B-D).

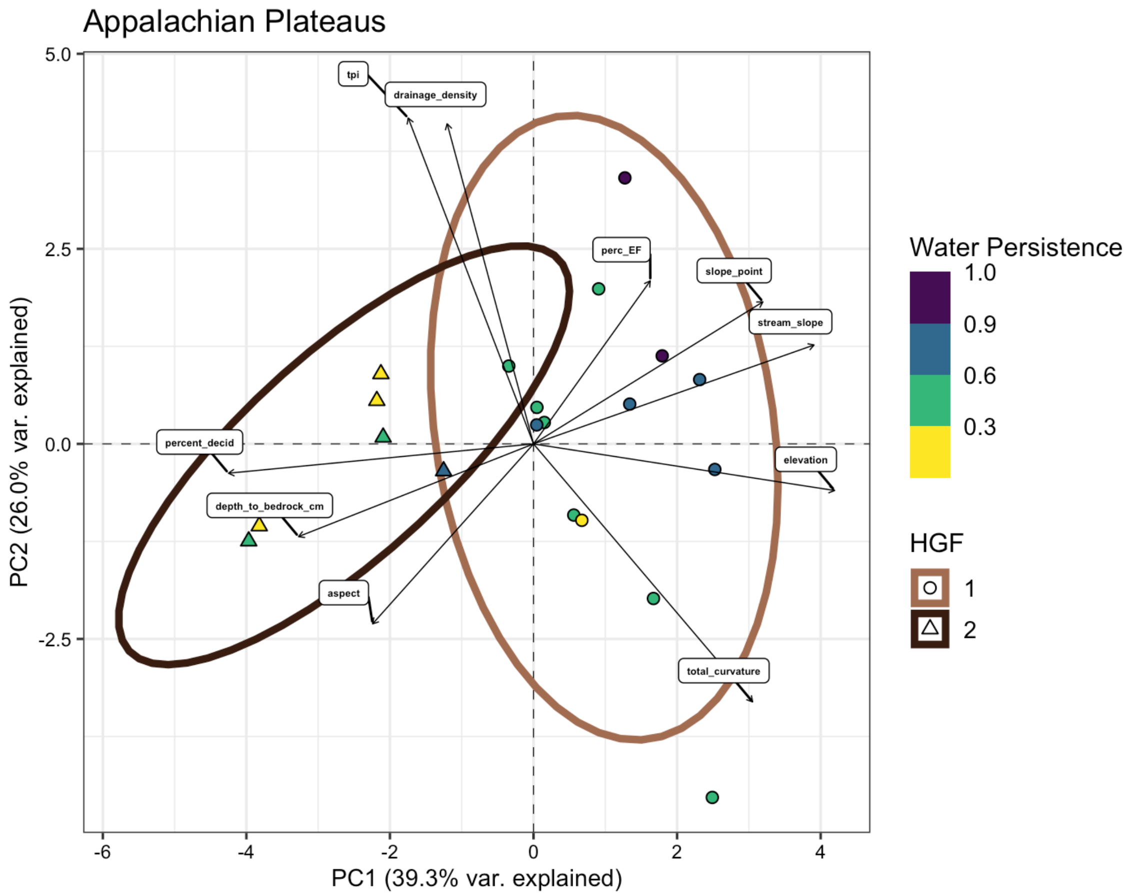

Figure S13. Principal Components Analysis of physiographic variables in the Appalachian Plateaus, with delineated HGFs marked by point shapes. Variables were subsetted from Table S1, such that all correlated variables (Pearson's correlation > |0.8|) were removed. Ellipses indicate HGF group spread, and points are colored by water persistence.

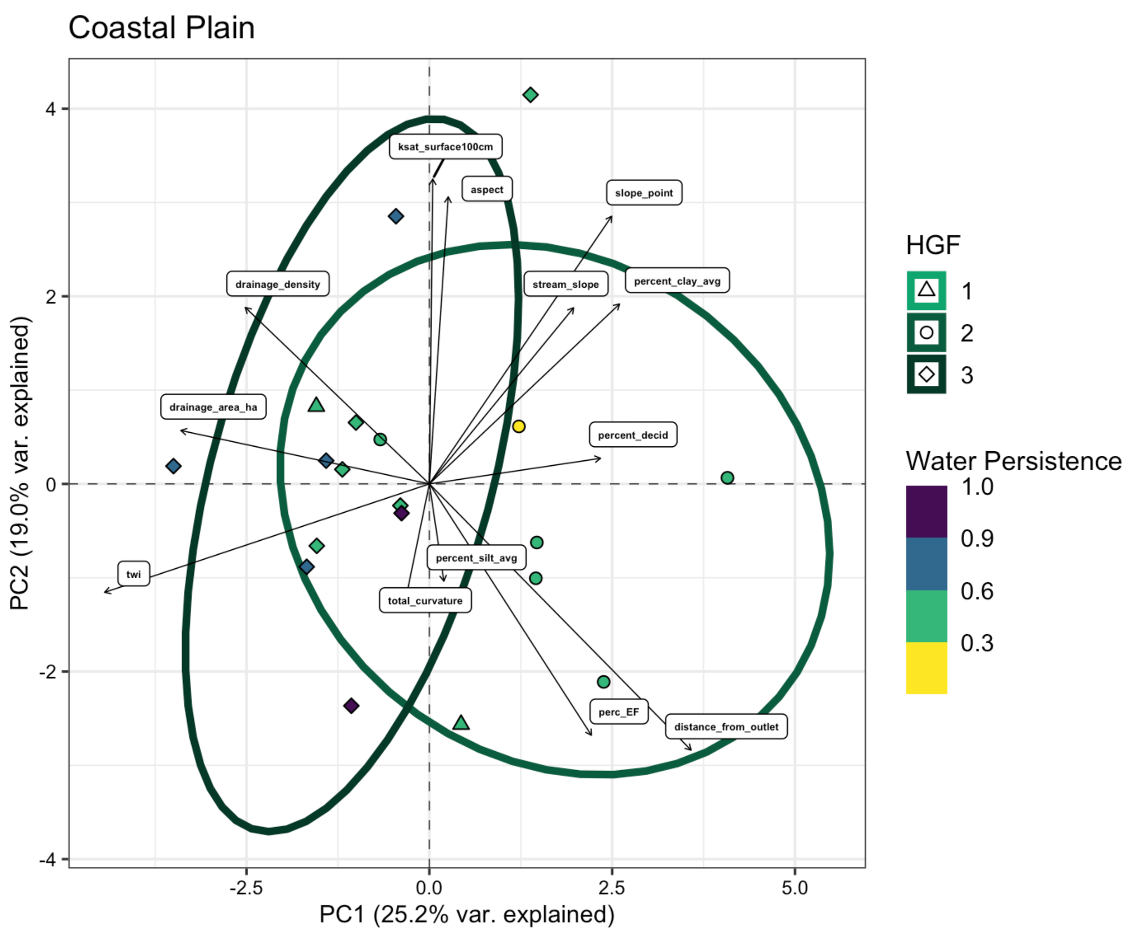

Figure S14. Principal Components Analysis of physiographic variables of the Coastal Plain, with delineated HGFs marked by point shapes. Variables were subsetted from Table S1, such that all correlated variables (Pearson's correlation > |0.8|) were removed. Ellipses indicate HGF group spread, and points are colored by water persistence.

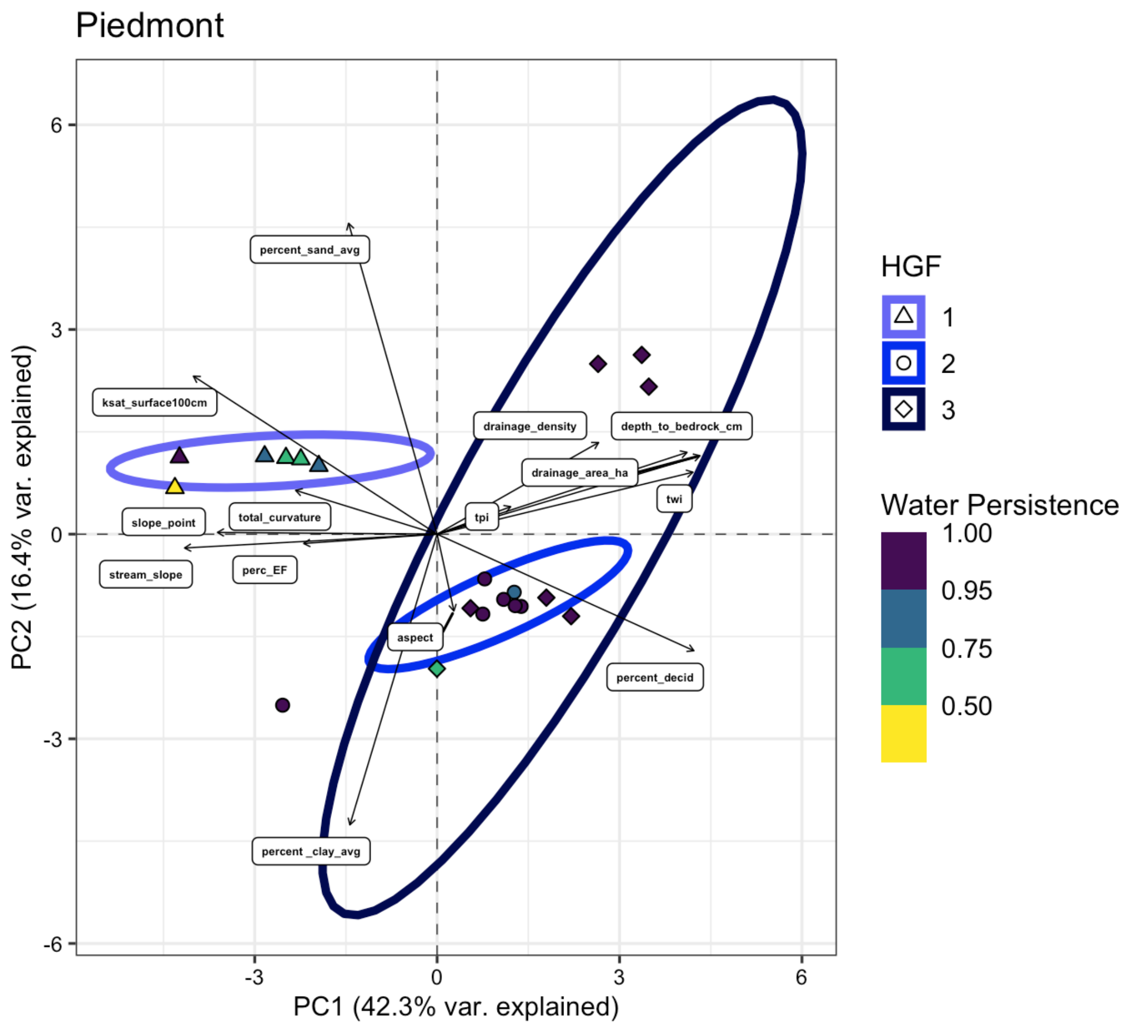

Figure S15. Principal Components Analysis of physiographic variables in the Piedmont, with delineated HGFs marked by point shapes. Variables were subsetted from Table S1, such that all correlated variables (Pearson's correlation > |0.8|) were removed. Ellipses indicate HGF group spread, and points are colored by water persistence.

References

Alabama Historical Commission. (2002). The History of Agriculture in Alabama: A Historic Context. Retrieved from https://ahc.alabama.gov/architecturalprogramsPDFs/History%20of%20Agriculture%20in%20Alabama.pdf

Chescheir, G. M., Nettles, J. E., Youssef, M., Birgand, F., Amatya, D. M., Miller, D. A., et al. (2018). Optimization of Southeastern Forest Biomass Crop Production: A Watershed Scale Evaluation of the Sustainability and Productivity of Dedicated Energy Crop and Woody Biomass Operations (No. DOE-NCSU--04395). North Carolina State Univ., Raleigh, NC (United States). https://doi.org/10.2172/1437923

Cook, T. A. (1982). Stratigraphy and structure of the central Talladega slate belt, Alabama Appalachians. In D. N. Bearce, W. W. Black, S. A. Kish, & J. F. Tull (Eds.), Tectonic Studies in the Talladega and Carolina Slate Belts, Southern Appalachian Orogen (p. 0). Geological Society of America. https://doi.org/10.1130/SPE191-p47

Dobbs, N. A. (2016). Hydrology and Water Quality Dynamics in Coastal Plain and Upland Watersheds with Loblolly Pine (Pinus taeda) and Switchgrass (Panicum virgatum) Intercropping in the southeastern United States. Retrieved from http://www.lib.ncsu.edu/resolver/1840.20/33346

Fickle, J. (2014). Green Gold. Retrieved June 20, 2025, from https://www.uapress.ua.edu/9780817318130/green-gold/

Florinsky, I. V. (2016). Chapter 1 - Digital Terrain Modeling: A Brief Historical Overview. In I. V. Florinsky (Ed.), Digital Terrain Analysis in Soil Science and Geology (Second Edition) (pp. 1–4). Academic Press. https://doi.org/10.1016/B978-0-12-804632-6.00001-8

Griffith, G. E., Omernik, J. M., Comstock, J. A., Lawrence, S., Martin, G., Goddard, A., et al. (2001). Ecoregions of Alabama. U.S. Environmental Protection Agency, National Health and Environmental Effects Research Laboratory, Corvallis, OR.

Kidd, R. E., & Lambeth, D. S. (1995). HYDROGEOLOGY AND GROUND-WATER QUALITY IN THE BLACK BELT AREA OF WEST-CENTRAL ALABAMA, AND ESTIMATED WATER USE FOR AQUACULTURE, 1990 (Water-Resources Investigations Report No. 94–4074). Tuscaloosa, Alabama: U.S. Geological Survey. Retrieved from https://web.archive.org/web/20190501065314id_/https://pubs.usgs.gov/wri/1994/4074/report.pdf

Lindsay, J. B. (2016). Whitebox GAT: A case study in geomorphometric analysis. Computers & Geosciences, 95, 75–84. https://doi.org/10.1016/j.cageo.2016.07.003

Sapp, C. D., & Emplaincourt, J. (1975). Physiographic regions of Alabama. Geological Survey of Alabama. Retrieved from https://ngmdb.usgs.gov/Prodesc/proddesc_55813.htm

Szabo, E. W., Osborne, W. E., Copeland, C. W., & Neathery, T. L. (1988). Geologic map of Alabama. Geological Survey of Alabama. Retrieved from https://ngmdb.usgs.gov/Prodesc/proddesc_55859.htm

Trimble, S. W. (2008). Man-Induced Soil Erosion on the Piedmont, 1700-1970 (2nd ed.). Ankeny, IA: Soil and Water Conservation Society.

Wahl, K. D. (1966). Geology and ground-water resources of Greene County, Alabama. Geological Survey of Alabama. Retrieved from https://ngmdb.usgs.gov/Prodesc/proddesc_55588.htm

Wilson, J. (2018). Calculating Land Surface Parameters. In Environmental Applications of Digital Terrain Modeling (pp. 53–149). John Wiley & Sons, Ltd. https://doi.org/10.1002/9781118938188.ch3